

中国激光

极紫外探测器的研究进展

郑伟*, 张乃霖, 朱思琪, 张利欣, 蔡炜

中山大学光电材料与技术国家重点实验室, 中山大学材料学院, 广东 深圳 518107

摘要 极紫外探测器在电子工业、空间探索、基础科学等领域有着无法替代的作用。本文综述了不同类型极紫外探测器的优势及研究进展, 包括气体探测器、闪烁体、微通道板以及半导体极紫外探测器, 重点介绍了具有优异抗辐照能力的宽禁带半导体极紫外探测器及其潜在的应用优势。最后, 本文展望了极紫外探测器在耐辐照功率监测、高分辨率成像和高抑制比极紫外微光探测等方面的应用前景, 并指出了其面临的主要挑战。

关键词 探测器; 极紫外; 闪烁体; 气体探测器; 宽禁带半导体探测器

中图分类号 O439

文献标志码 A

DOI: 10.3788/CJL231569

1 引言

极紫外(EUV)光是指电磁波谱中波长介于10 nm到120 nm的电磁辐射。随着现代科学技术的发展和进步, 极紫外探测器在电子工业、空间探索、基础科学等领域展现出越来越大的应用潜力^[1-2]。

在电子工业领域, 现代集成电路精密制造已成为推动极紫外探测器发展的主要动力。集成电路制造对更高集成度的需求日益增长, 主流的深紫外光刻技术(如193 nm浸没式光刻)正逐渐接近其物理极限。极紫外光刻技术使用波长短至13.5 nm的极紫外光在硅片上制作更小的电路图案^[3], 为超大规模集成电路提供更小的器件单元, 如图1(a)所示。在极紫外光刻系统中, 利用高能激光轰击锡(Sn)液滴, 将Sn加热至极高温度形成高温等离子体, 从而激发出波长为13.5 nm的极紫外光^[4-5], 如图1(b)~(c)所示。在曝光过程中, 极紫外辐射剂量及其稳定性直接影响着整个制程的效率和最终产品的良率。因此需要性能可靠的功率计对极紫外光源功率以及曝光剂量进行精确的实时监测^[6-8]。

另外, 极紫外光刻掩模版的纳米尺度缺陷检测是集成电路制造领域的另一重要需求。极紫外光刻掩模版通常由衬底上沉积的多层介质反射膜构成, 薄膜上局部凸起或凹坑形成的相位缺陷会削弱反射光的强度, 进而影响掩模区域的投影图像^[9]。这种相位缺陷一般在纳米尺度^[10], 超出了普通光学显微镜的观测能力。随着极紫外光源以及成像技术的发展, 13.5 nm极紫外显微镜已经被成功开发并被应用于掩模的纳米缺陷检测^[9-12], 如图1(d)~(f)所示。其核心部件之一是

具有成像能力的极紫外探测器。

在空间探索领域, 极紫外辐射探测可用来研究太阳活动和星际物质的演化。太阳的极紫外辐射与太阳活动紧密相关。尤其是太阳耀斑和日冕物质抛射等太阳风暴事件, 其往往伴随着大量极紫外辐射的发射, 是地球空间环境的重要破坏因素^[13]。人们可以通过对太阳极紫外辐射的监测来预报太阳风暴的形成和传播。图1(g)展示了用于太阳辐照监测的太阳动力学天文台(SDO)航天器的外观图^[14]。研究已表明, 极紫外辐射总能量与太阳风暴能量的变化规律是相符的^[14], 如图1(h)所示。太阳极紫外辐射的光谱由数千条发射线和一些连续线组成, 主要从太阳的色球层、过渡层和日冕层发射出来, 并且具有随时间变化的波长依赖性^[14], 如图1(i)所示。极紫外探测技术在监测和理解上述太阳活动方面起着关键作用, 能够提供关于太阳耀斑等动态天文事件演化过程的重要数据, 从而使人们可以更好地理解太阳活动如何影响地球空间环境以及预测空间天气, 进而保护地球以及人类太空活动。此外, H 和 He 元素是星际物质的主要组成元素, 并且它们在极紫外光谱区域的截面最大, 这使得极紫外探测成为研究星际物质最有效的工具之一。通过对星际物质进行极紫外探测, 科学家们可以重建遥远星际区域的极紫外光谱, 为研究星际物质的性质和星际辐射的产生提供重要参考^[14-17]。

在基础科学领域, 极紫外探测技术已经成为科学家探索微观世界的重要工具, 并为未来的科学探索开辟了新的研究途径。极紫外探测技术已被广泛应用于高能物理^[18]、量子电动力学^[19]、非线性光学等多个学

收稿日期: 2023-12-25; 修回日期: 2024-03-15; 录用日期: 2024-03-18; 网络首发日期: 2024-04-05

基金项目: 国家自然科学基金(62374186)、广东省自然科学基金-杰出青年项目(2021B1515020105)

通信作者: *zhengw37@mail.sysu.edu.cn

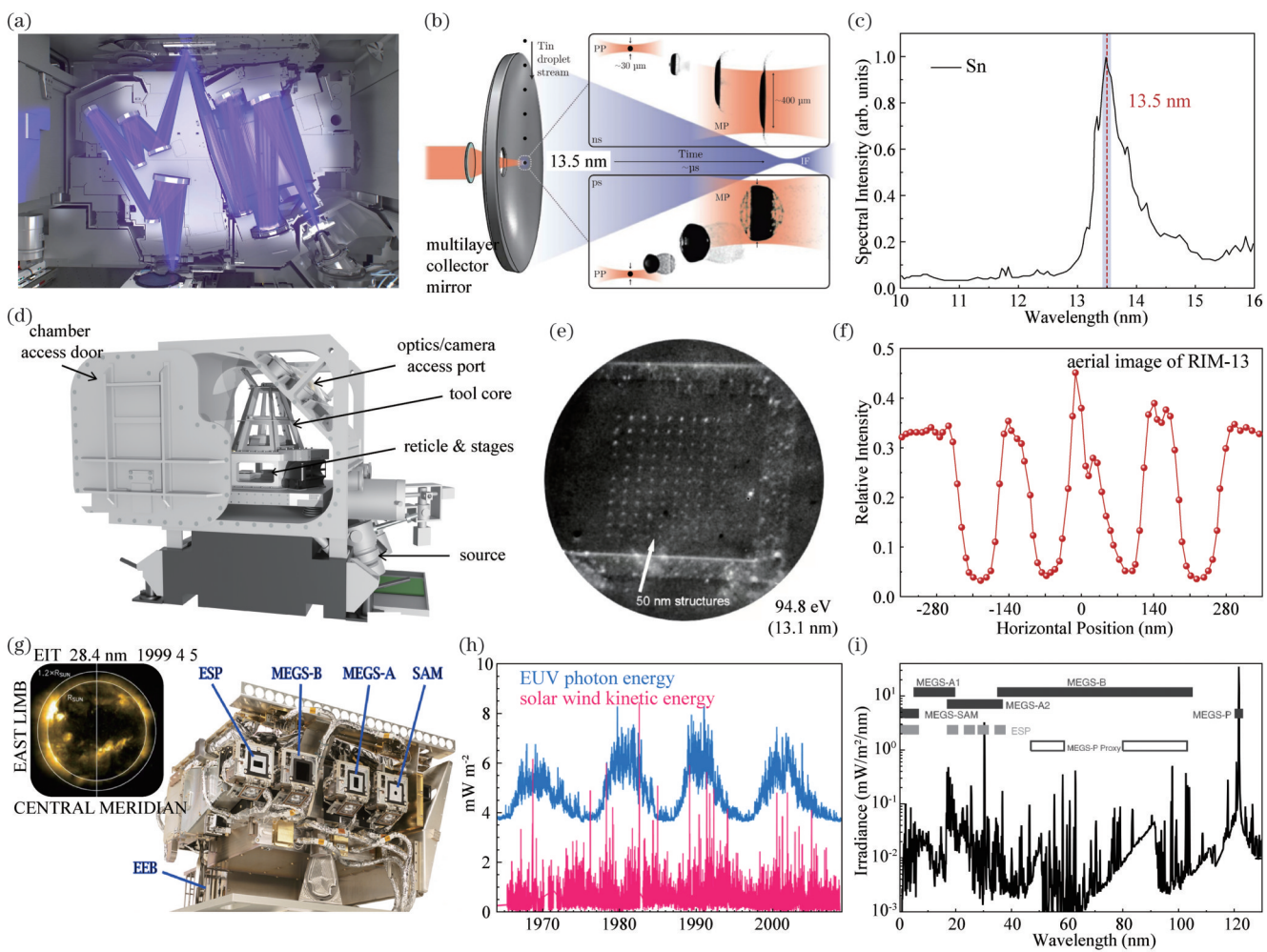


图 1 极紫外探测器在电子工业制造和空间探索领域的应用。(a)极紫外光刻系统示意图^[3];(b)典型工业极紫外光源模块中激光-液滴相互作用的简化原理图^[4];(c)Sn在极紫外波段的发射光谱^[4];(d)极紫外反射组件的光学系统及其机械设计图;(e)极紫外成像检测小于50 nm的缺陷结构^[11];(f)由极紫外显微镜在RIM-13中生成的掩模版的高度起伏;(g)用于开发太阳辐照预报能力的太阳盘以及太阳动力学天文台(SDO)航天器的外观图^[14];(h)波长小于120 nm的极紫外光子的每日总能量与太阳风粒子的能量对比^[14];(i)各种极紫外线变化实验仪(EVE)的波长覆盖范围与2008年4月14日原型EVE仪器获得的太阳最小光谱对比^[14]

Fig. 1 Application of the extreme ultraviolet (EUV) photodetector in electronics manufacturing and space exploration. (a) Schematic diagram of EUV lithography system^[3]; (b) simplified schematic diagram of laser - droplet interaction in a typical industrial EUV light source module^[4]; (c) emission spectrum of Sn in EUV wavelength range^[4]; (d) optical system and mechanical design cross-section of EUV reflective components; (e) defect structures smaller than 50 nm of the EUV imaging detection^[11]; (f) height fluctuation of a mask generated by an EUV microscope in the RIM-13 tool; (g) appearance of the solar disk and the SDO spacecraft used for developing solar irradiance forecasting capabilities^[14]; (h) a comparison between the daily total energy of EUV photons with a wavelength shorter than 120 nm and the energy of solar wind particles^[14]; (i) a comparison between the wavelength coverage ranges of various extreme ultraviolet variability experiment (EVE) instruments and the solar minimum spectrum obtained by the prototype EVE instrument on April 14, 2008^[14]

科,为各领域的科学提供了有力的技术支持,推动了这些领域的知识和技术进步^[20]。极紫外光可以通过同步辐射、自由电子激光(FEL)、等离子体发射以及各类气体放电辐射来获得^[21-24],这些光源的深入开发促进了各类基础科学的进步。例如,极紫外光^[25]可以在聚合物表面生成微米和纳米结构,从而改变聚合物生物材料的表面特性,实现对生物相容性的精确控制^[26]。此外,极紫外光具有穿透力低以及空间分辨率高和相

位对比度优势,为生命科学研究提供了新的工具和方法。采用极紫外光照射单个细胞获得其衍射图案,研究者们可以区分不同类型的乳腺癌细胞^[27]。同时,极紫外光可以用于对微生物样品进行无标记的高分辨率化学敏感成像^[28]。然而,基础研究的准确性与极紫外光强的精确标定密切相关,因此迫切需要研制专门针对极紫外波段的标准探测装置,以便对极紫外光的波长和绝对强度进行精确测量。

上述不同的应用场景对极紫外探测技术提出了不同的性能要求。极紫外光具有波长短、光子能量高、传播需要真空环境等特点,导致极紫外探测不能借助传统的光学材料、仪器和方法实现,这使得极紫外探测的研究工作面临着特殊的技术挑战。随着现代科学与技术的进步,极紫外探测技术也取得了长足发展,科研人员已经广泛研究并开发了基于不同探测介质和工作机制的极紫外探测器,包括气体探测器、闪烁体、微通道板和半导体探测器等。

气体探测器通过检测气体分子吸收极紫外辐射后的电离过程来获取极紫外辐射信息,具有长期稳定性和实时监测光子通量的优势,常被用于大科学装置中大功率极紫外光源(例如同步辐射和 FEL)的标定。极紫外闪烁体是一种基于下转换效应的探测器,能将不可见的极紫外光转换成可见光从而被后端的光电二极管或者光电倍增管收集,可用于极紫外高速探测和成像。微通道板是一种基于外光电效应的高增益电子倍增器件,其将极紫外光子转化为电子,输出的是二维电子图像,已被广泛应用于航天活动的探测任务中。半导体探测器是一种基于内光电效应的低功耗微型探测器,包括硅和宽禁带半导体探测器,具有体积小、重量轻、易于集成等优点。硅探测器具有成熟的制造工艺,已成为极紫外检测领域的标准探测器。但是,由于硅的带隙较小,硅探测器的极紫外辐射损伤阈值低^[29]。在高通量极紫外辐照下,硅的强吸收导致的热效应以及其他非线性光学效应会加速器件的老化,缩短器件的使用寿命。宽禁带半导体极紫外探测器具有更高的辐照损伤阈值^[30],近年来受到广泛关注。相对于硅极紫外探测器,在同等的辐照条件下,宽禁带半导体极紫外探测器具有更长的使用寿命。接下来本文将分别介绍上述气体探测器、闪烁体、微通道板和半导体探测器在极紫外探测方面的发展与研究现状,重点关注宽禁带半导体极紫外探测器。

2 极紫外探测器的发展与研究现状

2.1 气体极紫外探测器

气体探测器(GMD)的工作原理基于气体原子的光电离。入射的极紫外辐射导致高压电极和收集电极之间的气体发生电离,电离产生的离子和电子被均匀的静电场分离并完全提取出来,最终在收集电极上形成电脉冲输出^[31-32],如图 2(a)所示。对于同步辐射以及 FEL 等大功率和强辐射极紫外光源,标定其极紫外绝对光子通量对于后续的定量测量来说必不可少。图 2(b)展示了基于不同稀有气体工作介质的 GMD 检测下限^[33],可以看出氙气更适合作为极紫外波段的探测气体。图 2(c)和图 2(d)分别是 Sorokin 研究团队以氙气为探测气体测量得到的脉冲信号^[34],以及 Xe^{2+} 和 Xe^{3+} 离子的飞行时间。尽管绝对光子通量一般由半导体光电二极管测量得到,然而,强极紫外辐射脉冲可能

会使半导体光电二极管饱和、退化,甚至毁坏^[35],进而使得极紫外探测的不确定性增大。GMD 可以克服辐射引起的探测器性能退化,并且允许实时监测光子通量,具有稳定性高和使用寿命长的优势,已被用于各种高强度、高脉冲极紫外光源的标定。Kirschner 等^[35]使用 GMD 对极紫外插入装置光束线的绝对光子通量进行了实时监测,并将得到的数据与光电二极管的测量值进行对比。结果显示,两者的偏差低于 5%,如图 2(f)所示。

GMD 技术的发展较早,早在 1964 年,Samson^[36-37]就使用双电离室的 GMD 测量了真空紫外(VUV, 10~200 nm)的辐射绝对强度。随后,Saito 等^[38-39]将其应用到同步辐射中对软 X 射线的绝对强度进行测量。然而,由于双电离室的高气压气体会大量吸收光子束,GMD 不适合用于在线监测光子强度^[40]。2003 年,Richter 课题组^[33-34]开发了一种新型的 GMD,其基于低粒子密度下稀有气体的原子光电离和法拉第杯对光子和光电子的电荷进行监测,降低了对光子的吸收,可用于对 FEL 的 VUV 辐射进行脉冲分辨测量。德国的 FLASH 是世界上第一台 FEL,其将 GMD 作为光子诊断系统的永久组成部分。Richter 课题组^[41]开发的 GMD 在 FLASH 上实现了光子脉冲能量的测量不确定度优于 10%,光子束位置的测量不确定度低于 20 μm,时间分辨率优于 100 ns。

GMD 的另一种应用是将气体光电离室与飞行时间质谱仪结合,也被称为光电离分光计或光电离光谱仪。1981 年,Bobashev 等^[42]研制了可用于 0.1~100 nm 辐射的光电离分光计,其已被用于激光等离子体实验中 VUV 和软 X 射线辐射的测量。针对 FEL 中自放大自发辐射过程的随机性问题,升级的 FLASH 2 装配了用于测量气体光电离产生的电子和离子飞行时间光谱的光电离光谱仪(OPIS),该光谱仪可以实现单束分辨率的在线波长监测,如图 2(e)所示^[43]。

此外,在过去的 10 年中,研究人员还将 GMD 技术扩充到硬 X 射线光谱范围。到 2017 年,GMD 已经安装在多个 FEL 装置(FLASH 2、SwissFEL、Europeam XFEL、LCLS II)上,为实验人员提供永久服务^[44-48]。2019 年,Sorokin 等^[40]在前期研究的基础上开发了一种新型 GMD,它可以在涵盖 VUV、EUV 以及软硬 X 射线的宽光谱范围内测量 FEL 绝对光子脉冲能量和光子束位置。该 GMD 可以实现优于 200 ns 的时间分辨率。

2.2 极紫外闪烁体

在极紫外波段,闪烁体对极紫外光的表征和成像具有重要作用。有效的极紫外闪烁体需要具备如下关键特性:高光产额、大尺寸、明确的产额对辐射特性的依赖性(例如已知的产额与辐射强度的函数关系)、快响应、高吸收系数以及高损伤阈值^[49]。目前,在极紫外探测领域关注较多的闪烁体有掺铈的钇铝石榴石

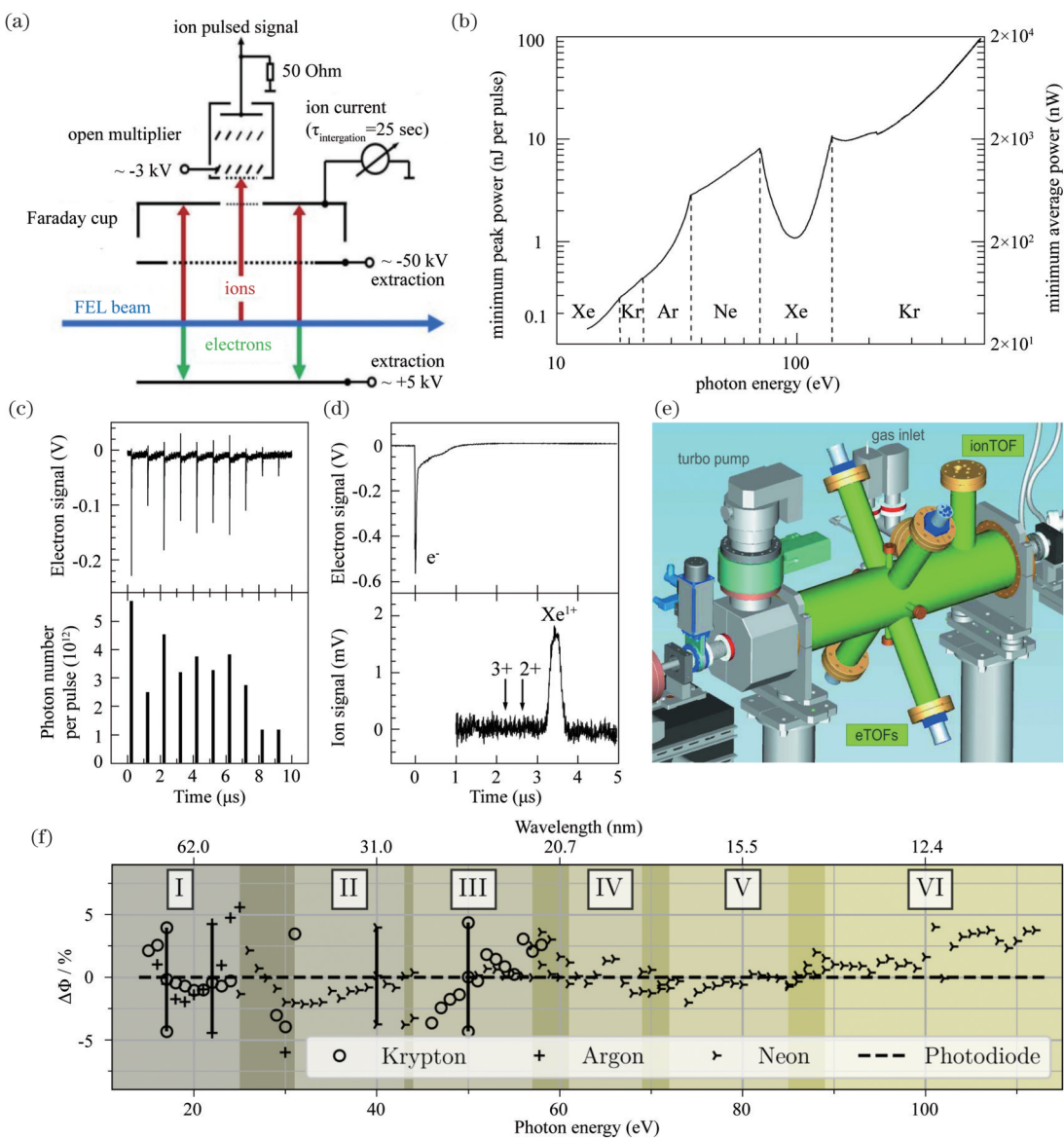


图2 气体极紫外探测器的研究进展。(a)GMD的工作原理^[32];(b)各种稀有气体的GMD的检测下限^[33]; (c)~(d)测量氙气得到的脉冲信号以及Xe²⁺和Xe³⁺离子的飞行时间^[34]; (e)OPIS设备简化模型^[43]; (f)GMD测量的光子通量与光电二极管测量值的相对偏差^[35]

Fig. 2 Research progress of the gas EUV detectors. (a) Schematic diagram of the working principle of a gas monitoring detector (GMD)^[32]; (b) detection limits of the GMD for various rare gases^[33]; (c)–(d) pulse signals obtained by measuring xenon gas and the flight time for Xe²⁺ and Xe³⁺ ions^[34]; (e) simplified model diagram of the online photoionization spectrometer (OPIS)^[43]; (f) relative deviation between photon flux measured by GMD and that measured by the photodiode^[35]

(Ce: YAG)、氧化锌(ZnO)和水杨酸钠。其中,Ce: YAG 闪烁体具有高的荧光效率,是极紫外检测及成像系统中常用的闪烁体;ZnO 闪烁体具有超快的响应时间,可用于超快极紫外辐射脉冲监测;水杨酸钠闪烁体在极紫外波段具有恒定且较高的量子效率以及低成本等优点,被广泛用于极紫外辐射探测。

Ce: YAG 闪烁体的化学式是 Ce³⁺:Y₃Al₅O₁₂,其荧光效率高达 75%^[50],荧光寿命约为 70 ns。Ce: YAG 的发光峰值位于 500~600 nm,与硅光电二极管的灵敏光谱相匹配^[51]。目前,Ce: YAG 闪烁体已实现商业化。最常见的Ce: YAG 是 0.2%Ce: YAG,其中铈原子

取代了晶格中的部分钇原子。Bahrenberg 等^[52]设计了一种由微锥结构和涂层表面组成的Ce: YAG 闪烁板,其输出耦合效率是传统平面闪烁板的4倍多(在5~50 nm 波长范围内)。Ce: YAG 闪烁体已在多个极紫外检测和成像系统中得到了集成应用^[52-57]。例如:Szilagyi^[53]在2010年展示了一种以Ce: YAG 晶体作为快速闪烁体在纳秒时间尺度上进行极紫外光成像的新方法;得益于Ce: YAG 晶体的高空间分辨率,研究人员将基于Ce: YAG 闪烁体的超快极紫外摄影机用于球磁/天体物理喷射实验中^[57]。然而,Ce: YAG 闪烁体的光稳定性与余辉水平仍存在局限。Yang 等^[58]证

实了 Ce:YAG 的长余辉和缓慢的荧光恢复会显著影响数据采集的准确性。

氧化锌(ZnO)晶体也是极紫外探测领域一种优秀的闪烁体。水热法生长的 ZnO 晶体在超快极紫外闪烁体领域展现出了巨大的潜力。实验中已经观察到, 在 13.9 nm 极紫外光激发下,ZnO 晶体的响应时间仅为 1.1 ns, 发光波长为 380 nm^[59-61]。水热法生长的 3 英寸 ZnO 单晶^[59]如图 3(a)所示。图 3(b)和图 3(c)展示了 13.9 nm 极紫外光激发 ZnO 荧光的时间分辨荧光光谱, 其可用时间常数为 0.9 ns 和 2.3 ns 的双指数衰减进行拟合。ZnO 可用于光刻中纳秒级持续时间的极紫外光源的表征^[62]。通过掺杂引入荧光猝灭通道可进一步缩短 ZnO 闪烁体的响应时间^[63-67]。Yamanoi 等^[63,65]在 ZnO 生长过程中掺杂铁离子制备了 Fe:ZnO, 其荧光的上升时间和衰减时间常数分别小于 10 ps 和 100 ps。使用 Fe:ZnO 闪烁体测得定时电子器件和激光脉冲的定时抖动小于 70 ps^[63,65]。进一步地, 他们在生长过程中人为引入铟离子制备了 In:ZnO, 其衰减时间常数减小至 3.1 ps^[64,67]。该快响应时间使得 EUV-FEL 与其他激光系统的精确同步精度达到了 3 ps。进一步地, 该课题组研究了 ZnO 单晶作为极紫外激光诊断成像器件的空间分辨率, 并用极紫外激光捕获了 ZnO 的单次发射图像^[61,68-69]。结果表明, ZnO 在水平和垂直方向上的空间分辨率分别为 5.0 μm 和 4.7 μm。此外, 有研究显示 ZnO 的短发光寿命有助于提高空间分辨率。因此, 掺杂的 ZnO 晶体的空间分辨率研究是值得期待的^[68-69]。

水杨酸钠是一种有机闪烁体, 具有优异的荧光效率, 且制备简单。在 EUV 辐射下, 水杨酸钠在 420 nm 附近显示荧光, 并且在 50~350 nm 光谱范围内表现出恒定且较高的量子产率^[70], 已被广泛用于短波紫外辐射监测^[71-72]。早在 1969 年, Bruner^[73]就提出了一种测量薄屏晶体磷光绝对量子效率的方法, 该方法测得极紫外(30.4~121.6 nm)激发下水杨酸钠的绝对量子产率约为 45%, 但其会受到样品厚度和老化的影响。近年来, 水杨酸钠已被集成在 VUV 辐射探测系统中。2017 年, Iglesias 等^[74]使用水杨酸钠测量了氩气和氧气混合气体中低压微波等离子体的 VUV 辐射, 如图 3(d)所示。水杨酸钠发射荧光的强度与入射的 VUV 光子通量成正比, 可用来原位测量 VUV 绝对辐射^[75]。2023 年, Han 等^[76]开发了基于水杨酸钠的 VUV 辐射实时监测系统, 并使用各种滤光片比较了不同波长范围内的光子强度。该系统相对于传统的 VUV 光谱仪具有更紧凑的体积、更高的检测精度和更高的时间分辨率。然而, 水杨酸钠闪烁体具有吸湿性和老化效应, 这会使其长期工作后的量子效率降低。其中可能的原因是系统受到了环境(包括真空泵油)污染、紫外线辐照以及水蒸气的影响^[76]。目前, 水杨酸钠闪烁体已经实现了商业化^[77], 如图 3(e)所示。

Mcpherson 公司推出的水杨酸钠闪烁体产品的荧光效率约为 60% (40~300 nm 激发), 衰减时间为 7~12 ns^[77]。此外, 在洁净干式真空泵的真空系统中, 该产品荧光效率的时间稳定性很好, 可以稳定运行超过 20 年。

近年来, 具有氮空位中心的荧光纳米金刚石(FND)闪烁体在极紫外辐射探测和成像领域引起了较大关注。这种闪烁体具有优异的光稳定性、快的荧光衰减时间、高的量子效率和可靠性, 其在 344 nm 激发下的连续谱及其截面电镜(SEM)图像如图 3(f)所示^[58,78]。2020 年, 台湾同步辐射研究中心的 Lu 等^[79-80]首次证明了 FND 作为极紫外闪烁体的应用前景, 其在 0.86~200 nm 同步辐射源辐射激发下表现出在 550~750 nm 范围内几乎恒定的发射光, 并且发光强度在数小时内未见明显下降。他们使用 FND 探测器测量了 O₂ 电子跃迁吸收截面(110~200 nm), 并将测量结果与水杨酸钠闪烁体进行了比较, 结果显示差异小于 5%。2023 年, Yang 等^[58]通过电喷涂沉积方法制备了 FND 薄膜, 其在极紫外激发下发出明亮的红光。在此基础上, 他们开发了基于 FND 的成像装置, 并将该装置用于 50 nm 和 13.5 nm 同步辐射的光束诊断, 诊断空间分辨率为 30 μm^[58]。

2.3 微通道板极紫外探测器

微通道板(MCP)是一种大面积的高空间分辨光电倍增探测器。其工作原理与光电倍增管类似, 不同的是, 其不会受到必须使用透明窗口的限制(目前只能测试波长大于 110 nm 的光子), 在极紫外光谱学和二维成像中得到了广泛应用。虽然裸露的 MCP 在极紫外光谱区域的量子效率较低, 但是在 MCP 上沉积光阴极材料可以大幅提高系统的量子效率^[81]。极紫外光通过光阴极转化成光电子, 光电子进入 MCP 的输入端并与通道壁碰撞, 产生二次电子; 二次电子继续被内部高压电场加速并沿通道而下, 其与通道壁的额外碰撞还会产生更多的二次电子^[82-83]。微通道板的工作原理和截面分别如图 4(a)和图 4(b)所示。1983 年, Siegmund 等^[81]讨论了用于极紫外检测的 MCP、光阴极材料和读出方案。1987 年, Vallerga 等根据实验室结果对比了 MCP 和电荷耦合器件(CCD)的极紫外探测性能, 结果显示 MCP 在极紫外下是更好的弱光探测器^[84]。

在过去的几十年中, MCP 极紫外成像探测器技术取得了重大进展, 包括光阴极改进^[85]、微通道板结构优化^[83,86-88]以及图像读取加速^[89-90]。MCP 已经被广泛运用于空间探测中的极紫外探测。1992 年和 2000 年, 美国航空航天局(NASA)分别发射了 EUVE 卫星和 IMAGE 卫星, 它们搭载了基于楔条形阳极的 MCP 成像探测仪。这些探测仪器首次实现了对赤道面上等离子体层全球分布的获取, 并且在太阳扰动期间成功观测到了地球等离子体层的变化^[90-93]。中国

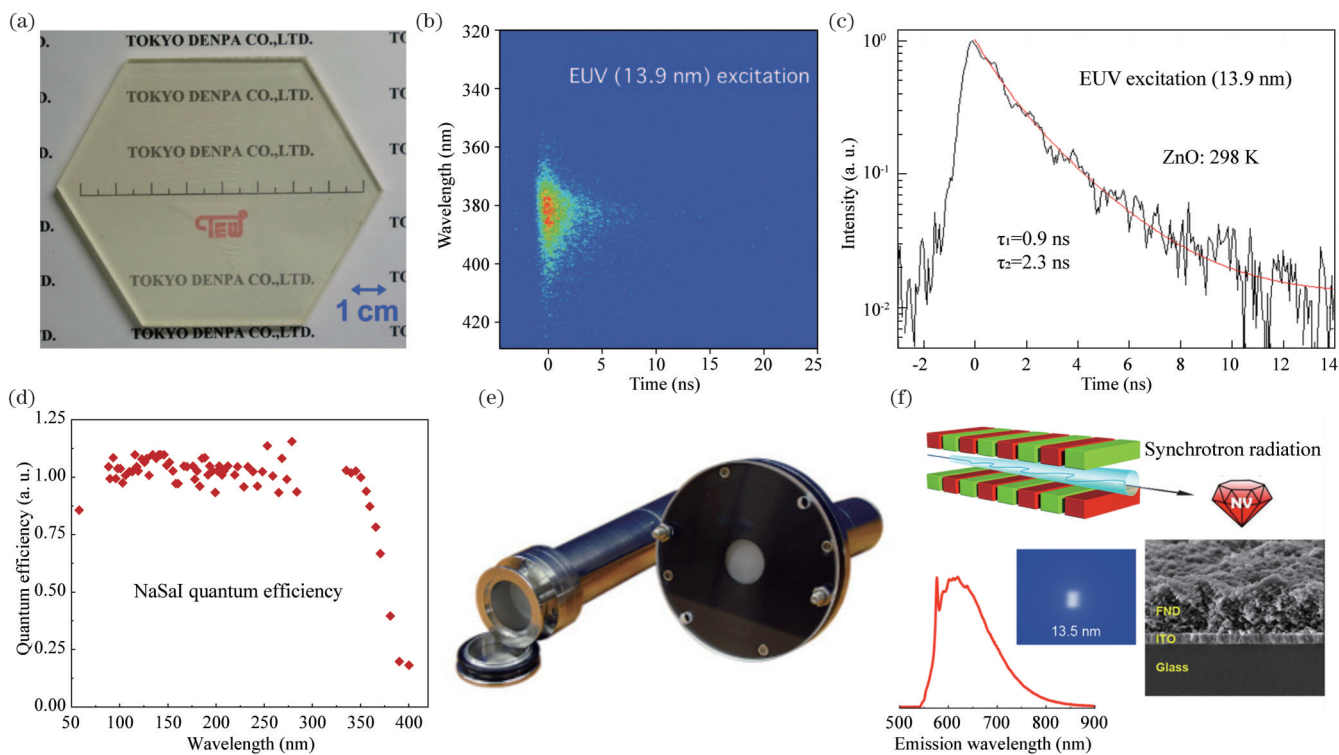


图3 极紫外闪烁体的研究进展。(a)ZnO闪烁体实物图^[59];(b)~(c)13.9 nm极紫外光激发ZnO的荧光时间分布,红色线为衰减拟合函数^[59];(d)水杨酸钠在50~400 nm光谱范围内的量子效率^[74];(e)水杨酸钠闪烁体产品^[77];(f)荧光纳米金刚石在344 nm光激发下的连续谱及其截面SEM图像^[58]

Fig. 3 Research progress of the EUV scintillators. (a) Photograph of ZnO crystal scintillator^[59]; (b)–(c) time distribution of ZnO fluorescence under excitation of EUV light at 13.9 nm, with the red line representing the decay fitting function^[59]; (d) quantum efficiency of sodium salicylate in the 50–400 nm spectral range^[74]; (e) product photograph of the sodium salicylate scintillator^[77]; (f) continuous spectrum and cross-sectional SEM image of the fluorescent nanodiamonds under 344 nm light excitation^[58]

科学院西安光学精密机械研究所的朱香平等^[94]对 MCP 极紫外成像探测器的性能进行了实验研究,为进一步提高 MCP 探测器空间分辨率和线性度提供了解决方案。中国科学院长春光学精密机械与物理研究所的尼启良课题组^[93,95]自主研制了二维 MCP 楔条形阳极光子计数成像探测器,该探测器由两片排列成 V 形的国产平面 MCP 堆及前端电路组成,具有 MCP 堆增益和空间分辨率高、暗计数率低及工作寿命较长等优异的性能,可以满足制备极紫外相机的要求。

其他集成 MCP 的系统还有宇宙热星际等离子体光谱仪(CHIPS)^[88]、轨道和可回收远紫外线和极紫外线光谱仪(ORFEUS)^[96]、世界空间天文台-紫外线(WSO-UV)天文卫星^[97]等。近年来,Siegmund 研究团队^[98-100]研制出了具有原子层沉积的新型硼硅酸盐玻璃 MCP,其具有良好的整体响应均匀性、较高的空间分辨率($<20 \mu\text{m}$)和低的背景($<0.05 \text{ event} \cdot \text{cm}^{-2} \cdot \text{s}^{-1}$)。其搭配新型碱卤化物光阴极,在宽波段下具有高的量子效率($\sim 60\% @ 115 \text{ nm} \& 65 \text{ nm}$)。该工作得到了 NASA 的支持,并且有望应用于 NASA 天文台的紫外探测系统,例如大型紫外/可见/红外探测卫星

(LUVIOR)和宜居系外行星天文台(HabEx)。

这些成就展示了极紫外 MCP 在空间探测领域取得的瞩目成绩。目前,用于极紫外探测的 MCP 已经实现了商业化,主要的产品供应商是 Hamamatsu 公司。Hamamatsu 公司通过增加开口率和选择合适的偏角极大地提升了微通道板的探测效率(如图 4(c)~(d)所示),同时通过采用较低的等效内阻(如 F6584 型号采用的等效内阻为 $2\sim 30 \text{ M}\Omega$)提高了最大线性输出及线性范围。此外,该公司还将 MCP 微通道的长度和直径等比例缩小,可在增大响应速度的同时不减弱增益(如 F4655-13 型号)。在实际应用中,Hamamatsu 公司还采用了将 2~3 片 MCP 叠在一起的反角设计,如此可使反馈离子难以进入第一级 MCP,有效减弱了离子反馈,提升了信噪比^[101]。

2.4 硅极紫外探测器

以上深入探讨了气体探测器、闪烁体和微通道板极紫外探测器及其应用场景,但是,它们特有的性质和工作条件(气体、高压)使得它们不适合应用在极紫外光刻领域。半导体探测技术凭借其小型化、易于操作、易于集成的优势推动着极紫外光刻技术不断向前发展。硅光电二极管的测试数据已经被作为极紫外

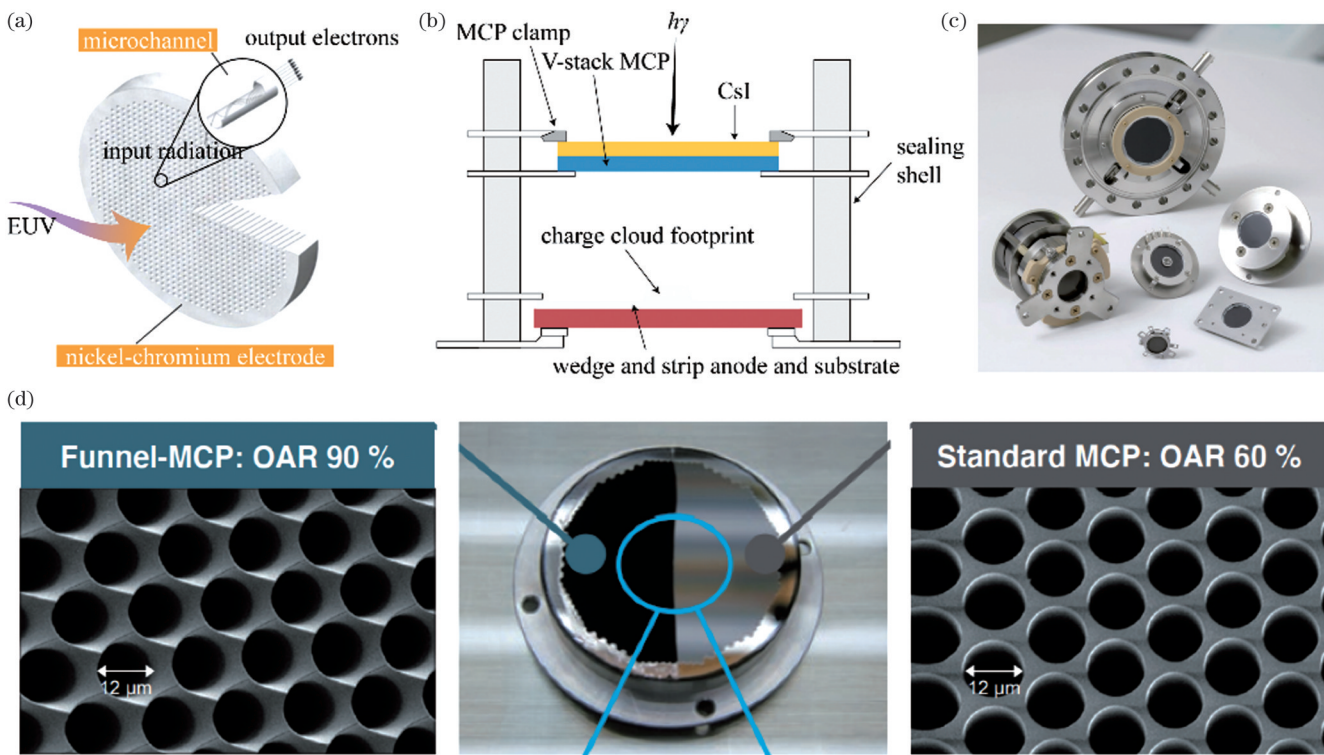


图 4 微通道板极紫外探测器的研究进展。(a)~(b)微通道板工作原理图;(c)Hamamatsu公司微通道板产品图^[101];(d)Hamamatsu公司通过选择合适的偏角提升了微通道板的探测效率^[101]

Fig. 4 Research progress of the microchannel plate detectors. (a)–(b) Schematic diagrams of the working principle of the microchannel plate; (c) product diagram of the microchannel plate from Hamamatsu Corporation^[101]; (d) Hamamatsu Corporation improved the detection efficiency of the microchannel plate by selecting an appropriate bias angle^[101]

区域的绝对校准标准^[102]。1990年,Canfield等^[103]对硅光电二极管开展了研究,其结构如图5(a)所示。用Ag和Al薄膜覆盖于器件表面滤波后的量子效率分别如图5(b)和图5(c)所示,实现了硅光电二极管极紫外探测器的窄带响应特性。1996年,Hartmann等^[104]通过在n-Si表面添加额外的p型注入来增加靠近表面的局部内建电场强度,提高了硅光电二极管极紫外探测器的电荷收集效率,使器件的性能有了一定提升。

然而,硅极紫外探测器的核心问题是辐射损伤造成的器件性能衰减。为了解决这一难题,科研人员在保证探测效率的同时对硅基极紫外探测器开展了提升耐辐照性能的研究。1993年,Korde等^[102]发现将硅光电二极管的二氧化硅层氮化后,其电离辐射耐受性有所提高。此外,硼掺杂的p型表面光敏层也被证明可以显著增强器件对极紫外辐照的耐受性。 \checkmark akić等^[105]在1~25 keV电子能量的照射下观察了具有硼掺杂层的硅光电二极管暗电流的衰减情况,在10 min内未发现器件发生较大的辐射损伤退化。Shi等^[106-107]使用纯硼化学气相沉积在硅基板上生长了Delta-like硼掺杂层,同时通过工艺调控使器件在13.5 nm波段的响应度接近理论值0.266 A/W(如图5(d)所示)。Aruev等^[108]发现在硅表面覆盖一层锆膜可以使器件具有更

高的抗极紫外辐射损伤能力,同时可以使器件对红光(633 nm)具有5个数量级以上的抑制。

经过长期的发展,硅探测器得益于其成熟的工业制造流程,在效率和成本方面具有显著优势。目前,商用硅极紫外探测器主要有Opto Diode公司生产的两种硅光电二极管:AXUV和SXUV。AXUV光电二极管可对0.0124~190 nm的光子、电子或X射线进行高性能测量。AXUV100G在极紫外区的响应度为0.15~0.26 A/W^[109],如图5(e)~(f)所示。SXUV系列极紫外增强型探测器具有较高的13.5 nm探测能力,在1~190 nm紫外线照射下具有稳定的响应度,这使其成为极紫外探测的理想选择。在有效面积均为10 mm×10 mm的情况下,SXUV的光响应度略低于AXUV^[109-110]。

2.5 具有潜力的宽禁带半导体极紫外探测器

在强辐射环境中,极紫外探测器需具备承受强烈辐射而不退化的优异性能。当前的硅半导体探测器在强辐射下易损伤,影响了其长期可靠性。因此,研究和开发对极紫外辐射具有高抗性的半导体材料是解决器件辐射损伤的关键。宽禁带半导体具有诸多优点,比如:1)具有较强的化学和物理稳定性,能够承受高能粒子的轰击而不发生晶格位移,从而可以大幅减少辐射引起的缺陷;2)具有较低的本征载流子

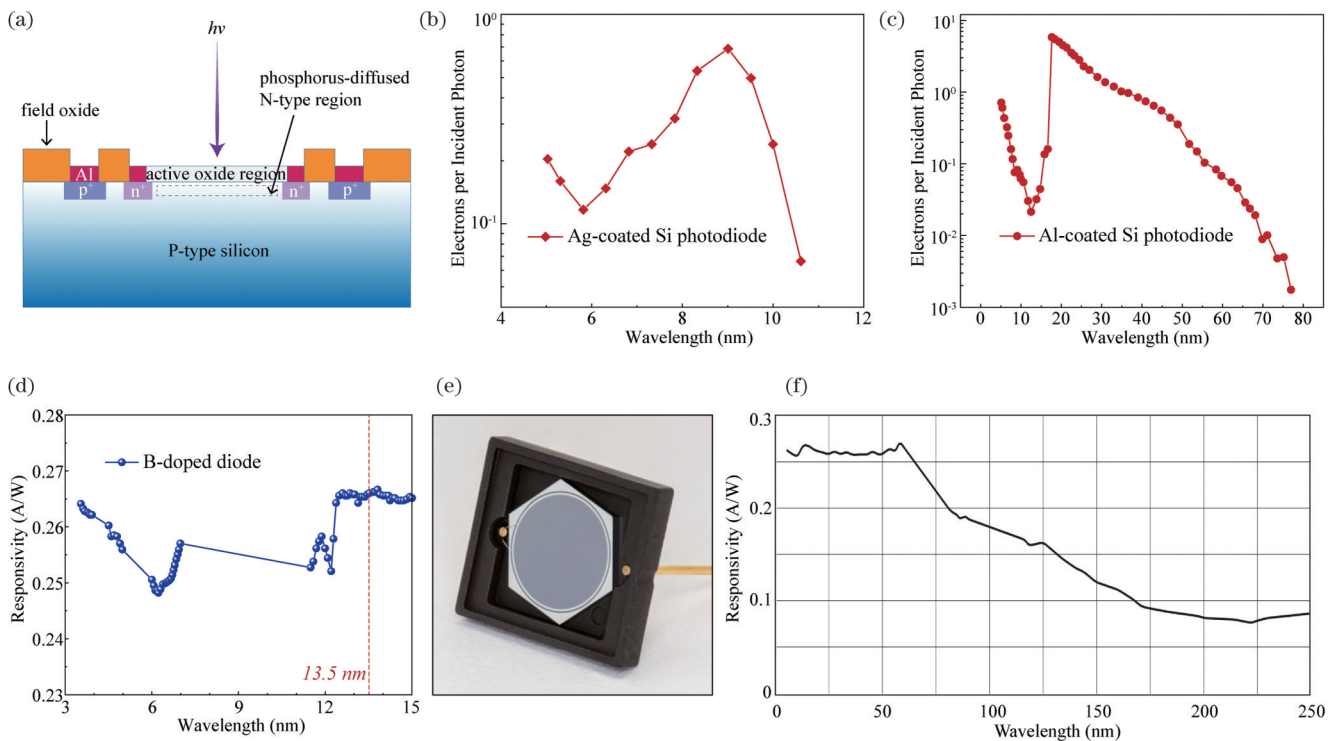


图 5 硅基紫外探测器的研究进展。(a) 硅光电二极管器件结构图^[103]; (b)~(c) 用 Ag 和 Al 薄膜覆盖于器件表面滤波后硅光电二极管的量子效率^[103]; (d) 硼掺杂硅光电二极管在 3~15 nm 波段内的光谱响应度^[106]; (e)~(f) AXUV 器件图及其在 0~250 nm 范围内的光谱响应度^[109]

Fig. 5 Research progress of the silicon-based EUV photodetectors. (a) Schematic diagram of the device structure of a silicon photodiode^[103]; (b)–(c) quantum efficiency of silicon photodiodes with Ag and Al thin films covering the device surface for filtering^[103]; (d) spectral responsivity of boron-doped silicon photodiodes in the range of 3 to 15 nm^[106]; (e)–(f) diagram of the AXUV device as well as its spectral responsivity in the range of 0 to 250 nm^[109]

浓度,当辐射诱导的载流子生成后,载流子复合的可能性较低,有助于维持高强度辐照下探测器的性能;3)能隙宽,因而具有更高的电子跃迁能量阈值,可以避免电子被热激发到导带形成的热噪声;4)对可见光波段不敏感,避免被可见光“污染”。正是由于这些优点,宽禁带半导体材料在制造耐高温及强辐射器件方面比传统的半导体硅材料更具优势,成为当前半导体技术向前迈进过程中备受关注的材料之一。接下来本文将详细介绍宽禁带半导体极紫外探测器的发展状况。

2.5.1 SiC 极紫外探测器

近年来,碳化硅(SiC)的单晶生长、外延生长以及离子注入等技术取得了巨大进步,采用这些技术可以制造 PIN 型^[111]、雪崩型^[112-113]、肖特基型^[114-115]器件。Torrisi 等^[116]展示了 SiC 探测器相较于传统硅探测器在探测效率上的显著优势,如图 6(a)所示。2005 年,Seely 等^[117]测试了 6H-SiC 光电二极管在 1.5~400 nm 波长范围内的响应度,测试结果如图 6(b)所示,该器件在极紫外波段的响应度约为 0.001~0.100 A/W。该工作虽然实现了 SiC 在极紫外波段的探测,但器件的性能并不理想。之后,科研人员从器件结构设计方

面着手,对 SiC 极紫外探测器的性能进行了提升,并通过选择不同的滤光层实现了不同波长范围的选择性响应^[118-119]。Gottwald 等^[120]使用铬电极制作了 4H-SiC 光电二极管,其在 70 nm 下的响应度约为 15.0 mA/W。Xin 等^[115]制备了 4H-SiC 肖特基结构的极紫外光电二极管,如图 6(c)所示。他们采用 10 nm 厚的镍和 7.5 nm 厚的铂作为半透明金属层,与 SiC 层形成肖特基接触,有效提高了器件收集载流子的能力。该器件在 21.5 nm 处的量子效率达到了 140%,这可能源于高能极紫外光子在此处电离产生了多个电子空穴对。Hu 课题组^[121]在 2 英寸 4H-SiC 晶圆上制造了 1×16 的 Pt/4H-SiC 肖特基光电二极管阵列,其在短于 61 nm 波长处的量子效率超过了 100%,在 10 nm 处达到了 10 e-/photon,如图 6(d)所示。南京大学的 Wang 等^[122]设计并制造了一种具有梯度掺杂诱导表面结的高性能 4H-SiC n-i-p 结构极紫外探测器。在光伏工作模式下,该探测器表现出了 0.104 A/W 的高响应度,在 13.5 nm 波长处具有接近理论极限的 960% 的量子效率,并且具有超低的漏电流和出色的光响应均匀性。该探测器的抗辐射性能也得到了初步验证,如图 6(e)~(f)所示。该工作展示了 SiC 极

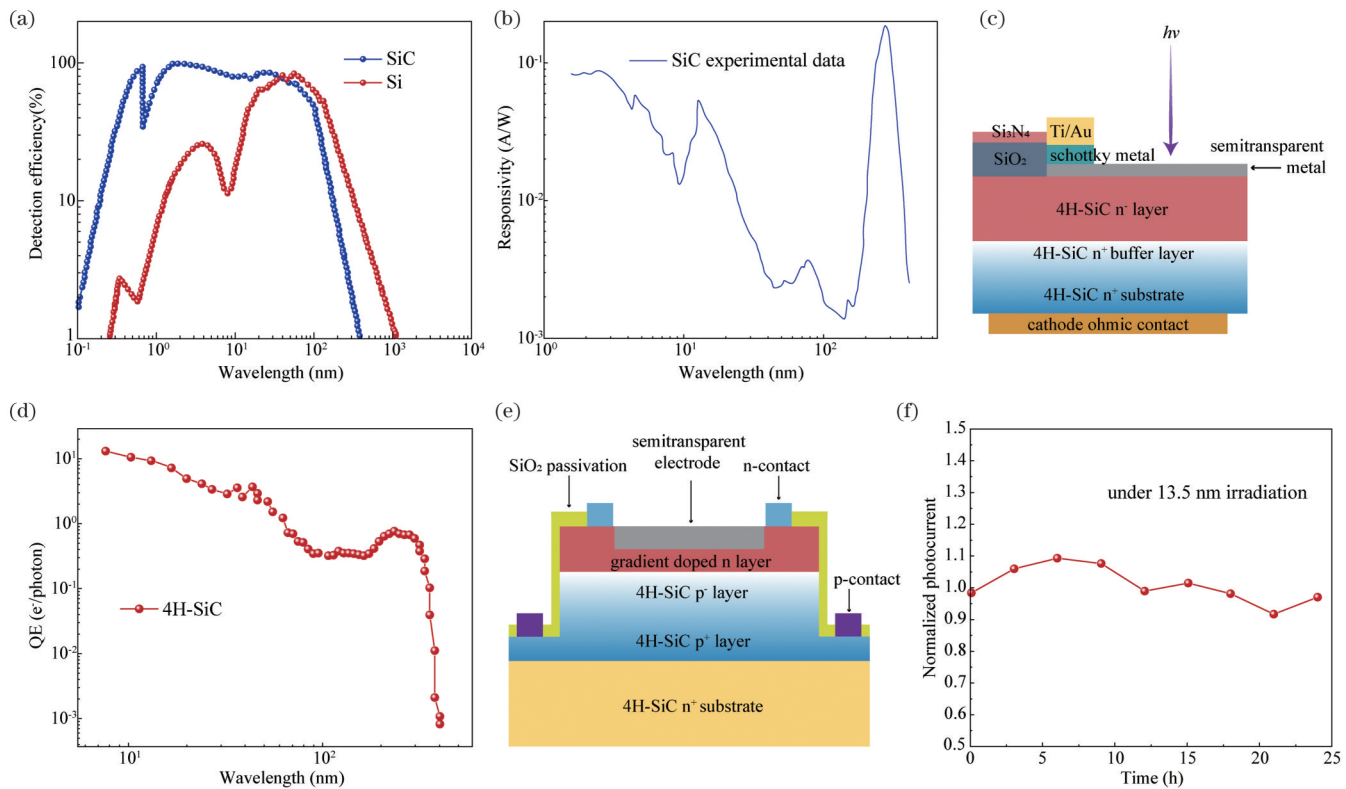


图 6 SiC 极紫外探测器的研究进展。(a)SiC 探测器与传统硅探测器的探测效率对比^[116];(b)6H-SiC 光电二极管在 1.5~400 nm 波长范围内的响应度^[117];(c)将半透明金属层作为肖特基接触金属结构的探测器结构图^[115];(d)1×16 的 Pt/4H-SiC 肖特基光电二极管阵列的量子效率^[121];(e)~(f)4H-SiC n-i-p 结构极紫外探测器的结构图及其辐照测试图^[122]

Fig. 6 Research progress of the SiC-based EUV photodetectors. (a) Comparison of detection efficiency between SiC detector and traditional Si detector^[116]; (b) responsivity of 6H-SiC photodiode in the wavelength range of 1.5 to 400 nm^[117]; (c) detector schematic using a semi-transparent metal layer as the Schottky contact metal structure^[115]; (d) quantum efficiency of a 1×16 Pt/4H-SiC Schottky photodiode array^[121]; (e)~(f) structure diagram of a 4H-SiC-based n-i-p junction EUV detector and its irradiance results^[122]

紫外探测器的发展潜力。厦门大学的 Zhang 等^[123]研制了双 P 层 4H-SiC p-i-n 结构极紫外探测器,其在 100 nm 处的响应度约为 75 mA/W。双 P 层结构可以有效减少光生载流子的复合,并在器件表面附近分离更多的电子空穴对。

2.5.2 AlGaN 极紫外探测器

AlGaN 是一种具有代表性的能隙可调的宽禁带氮化物材料。将 Al_xGa_{1-x}N 中的铝组分从 0 过渡至 1, 可使这些材料的带隙从 3.4 eV 变化到 6.2 eV, 对应于截止边缘从 365 nm 变化到 200 nm^[124]。近年来, AlGaN 在日盲紫外探测器上得到了应用。目前, 基于 AlGaN 的肖特基、金属-半导体-金属 (MSM)、PIN 结构的探测器已相对成熟^[125], 并在向短波紫外 (VUV、EUV) 波段拓展^[31]。2010 年, Malinowski 等^[126]制备和表征了 AlGaN-on-Si MSM 型极紫外探测器。为了避免硅的辐射吸收, 他们通过反应离子刻蚀对硅基底进行选择性刻蚀。这种背照式且有源层不会被金属电极遮蔽的方案可以提高极紫外探测器的灵敏度。类似的方法也可以用于肖特基二极管

及其二维阵列的制备, 肖特基二极管及其二维阵列的响应度如图 7(a) 所示^[127]。2011 年, Malinowski 等^[128]采用反向结构制备了 AlGaN-on-Si 肖特基光电二极管, 该反向结构可以有效减少表面载流子复合的损失。测试结果显示, 这种反向结构的光电二极管对极紫外光的灵敏度较高。分别在 58.4 nm 和 30.4 nm 波长处观察到了 He I 和 He II 特征发射线, 如图 7(b) 所示, 证明了使用反向层堆叠进行极紫外检测的可行性。

由于极紫外探测技术在光刻领域以及 FEL 等领域的应用需求不断增长, 器件的耐辐照性能逐渐成为研究人员需要考量的重要因素。Malinowski 研究团队^[129-130]对 AlGaN 极紫外探测器进行了抗辐照性能测试。他们使用波长为 13.5 nm 的高剂量极紫外辐射源, 测试了 AlGaN-on-Si 极紫外肖特基二极管响应度的衰减行为。结果显示: 在最高剂量约为 3.3×10¹⁹ photon/cm² 的极紫外辐射下, AlGaN 二极管没有发生明显的退化; 相比之下, 商用硅光电二极管在剂量为 2×10¹⁹ photon/cm² 的极紫外辐射下, 相对响应度下

降了 7%, 如图 7(c) 所示。

目前, 用于太阳观测的摄像头主要是硅基的 CCD 或互补金属氧化物半导体(CMOS)摄像头。虽然它们具有技术成熟度高和分辨率高的优势, 但它们也面临着辐射衰减和缺乏极紫外光谱选择性的困扰。随着集成光电技术的进步, AlGaN 焦平面阵列被制造出来。基于 AlGaN 的焦平面阵列探测器有可能实现高分辨率极紫外成像, 这种器件在高端工业、科学和航天应用等领域具有非常广阔的应用前景。阵列化的 AlGaN 探测器一般采用背照式结构, 可以进行倒装封装, 实现较高集成^[131]。然而, 极紫外的波长比衬底材料的截止波长短, 传统的背照式 AlGaN 探测器无法使用。因此, 需要对器件结构进行调整才能使 AlGaN 探测器的探测范围扩展到极紫外波段。事实上, 尽管穿过晶片进行倒装的正照式结构在理论上是可行的, 但背照式结构仍然是最实用的器件结构, 特别是具有小间距的阵列^[132]。目前的主流方法是在硅上异质外延 AlGaN 薄膜, 并减薄和刻蚀硅衬底^[126, 133]。Malinowski 等^[126, 134]对 AlGaN 材料外延生长、器件设计加工、封装集成和电

路读出等进行了细致研究, 制备了不同器件结构的 AlGaN 极紫外焦平面阵列成像仪。2010 年, 他们首次研制出了两种结构的 AlGaN-on-Si 极紫外成像仪^[134], 如图 7(d)~(e) 所示。该成像仪的背照式焦平面阵列大小为 256×256 , 像素间距为 $10 \mu\text{m}$, 器件可与专用硅基 CMOS 读出器结合。他们使用同步辐射进行了深紫外、远紫外和极紫外敏感性验证, 最低探测波长可达 1 nm 。2011 年, 他们基于上述反向肖特基结构制备了 $10 \mu\text{m}$ 像素间距的 256×256 探测器阵列, 并展示了使用波长低至 13 nm 的同步辐射获取的图像^[124, 127]。这些工作都是由 ESA-BOLD 项目支持的。此外, Reverchon 等^[132]也采用 AlGaN-on-Si 结构, 同时通过去除硅衬底并用干法刻蚀减薄 AlGaN 膜, 制备了 $30 \mu\text{m}$ 像素间距的 320×256 AlGaN 焦平面阵列。图 7(f) 显示了 AlGaN 焦平面阵列封装后的实物照片^[133], 该焦平面阵列在 $50 \sim 260 \text{ nm}$ 范围内的量子效率为 10%。AlGaN 材料在选择性响应和高辐射硬度方面的优势, 使得 AlGaN 极紫外成像仪在辐射检测领域具有广阔的应用前景。

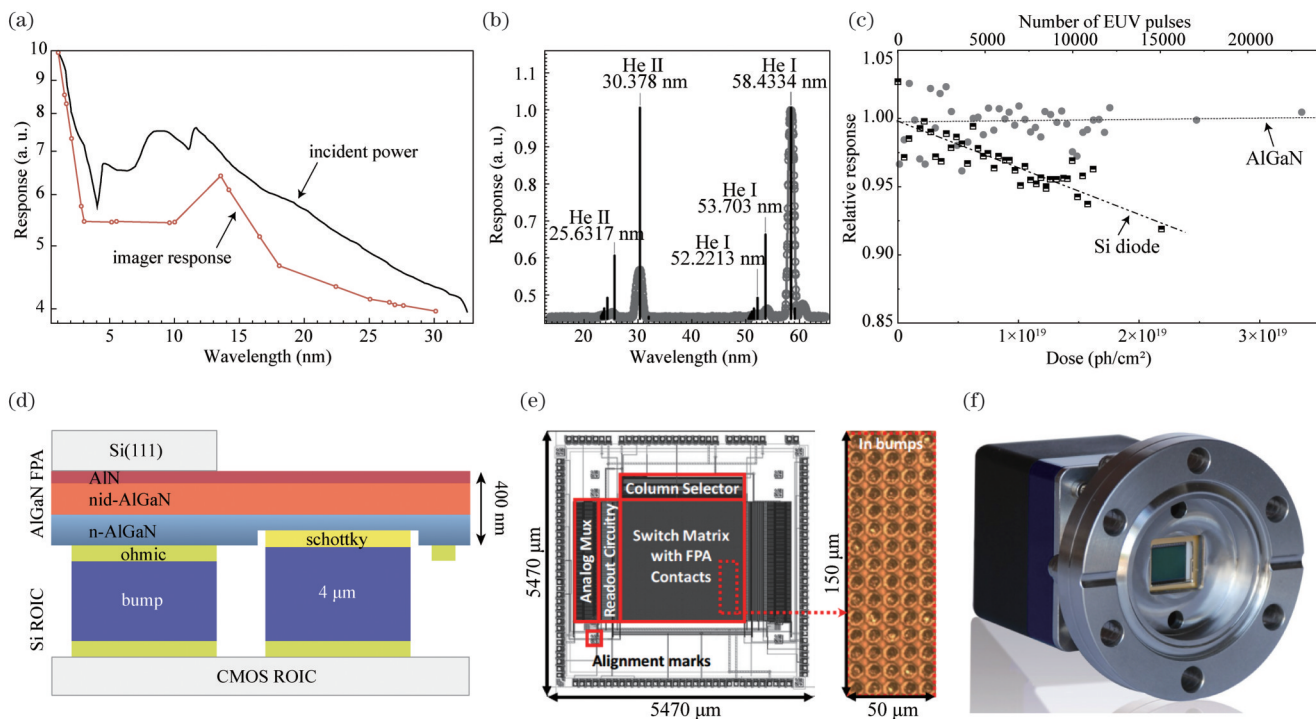


图 7 AlGaN 极紫外探测器的研究进展。(a) 对基底进行选择性刻蚀后的肖特基二极管及其二维阵列响应度^[127]; (b) 反向结构 AlGaN-on-Si 光电二极管在 58.4 nm 和 30.4 nm 波长处的 He I 和 He II 特征发射线^[128]; (c) AlGaN-on-Si 极紫外肖特基二极管和商用硅光电二极管的响应度衰减测试图^[130]; (d)~(e) AlGaN-on-Si 极紫外成像仪结构图^[134]; (f) AlGaN 焦平面阵列封装后的实物照片^[133]

Fig. 7 Research progress of the AlGaN-based EUV photodetectors. (a) Schottky diode and its two-dimensional array responsivity after a selective substrate etching^[127]; (b) characteristic emission lines of He I at 58.4 nm and He II at 30.4 nm in the reverse-structure AlGaN-on-Si photodiodes^[128]; (c) decay test chart of the responsivity of AlGaN-on-Si EUV Schottky diodes compared to commercially available silicon photodiodes^[130]; (d)–(e) structural diagrams of AlGaN-on-Si EUV imaging devices^[134]; (f) physical photograph of AlGaN focal plane arrays after packaging^[133]

2.5.3 金刚石极紫外探测器

金刚石是一种具有优异辐射硬度和化学惰性的超宽禁带半导体材料^[135]。基于金刚石的极紫外探测器在星载观测、光刻、光学研究、生物医学分析等领域同样具有潜在应用。随着极紫外探测技术在半导体制造领域的应用不断增加,人们对金刚石探测器在极紫外光谱范围内的性能进行了深入研究,包括金刚石探测器在极紫外光谱下的光电流响应、时间响应、探测效率,以及其在极紫外光源辐射下的稳定性和长期使用的性能衰减情况。

2000年,Pace等^[136]报道了意大利国家项目“极紫外金刚石探测器”获得的第一个结果。他们基于化学气相沉积(CVD)金刚石薄膜成功制备了叉指形光电导探测器,这些金刚石探测器在室温下具有极低的暗电流。罗马Tor Vergata大学的Balducci等^[137]通过改进的微波等离子体化学气相沉积设备在金刚石衬底上外延生长了150 μm厚高质量单晶金刚石薄膜,而后又进一步制备了光电导型器件。在极紫外光谱范围内,He II 30.4 nm以及He I 58.4 nm的发射线都能清楚地被该光电导型器件探测到,测得其在30.4 nm处的响应时间小于0.2 s。2009年,该实验室的AlmaViva等^[138]报道了基于p型半导体/本征半导体/金属(PIM)肖特基结构的CVD单晶金刚石极紫外探测器。由于二次电子发射会强烈影响极紫外区域的检测特性,他们将器件设计成三明治几何形状。测试结果表明该器件具有高均匀性和稳定性,在较低波长下显示出了较高的外量子效率。进一步地,该实验室开发了具有不同接触几何形状的PIM结构金刚石极紫外探测器,如图8(a)所示^[139]。其中:一种是横向几何结构,即在本征金刚石表面上制作半透明金属;另一种是平面结构,即在本征金刚石层表面制作叉指电极。两种器件均表现出了较低的暗电流以及优异的整流性能和响应可重复性。由于不同的操作配置,两种器件的响应度和量子效率在20~80 nm光谱范围内表现出相反的行为,如图8(b)所示。模拟结果表明,需要考虑金刚石-金属界面存在的一层薄薄的金刚石死区。因此,2011年,该实验室探究了不同整流金属接触材料的金刚石PIM器件在极紫外光谱区域的光谱响应性能^[140]。结果显示,除金接触外,银、铝、铬和铂接触材料的金刚石PIM器件的响应性在10 eV(124 nm)到60 eV(20.7 nm)能量范围内呈现出相似的趋势。拟合分析表明,金刚石死区需要被考虑,这很可能与光生载流子在金属电极附近的高复合有关,其会显著影响探测器的响应度。

用于太阳紫外观测的硅CCD存在辐射老化等难以克服的问题,金刚石材料可以避开这些限制,为开发高性能太阳望远镜和光谱仪提供了新途径^[141]。LYRA是一款太阳VUV辐射计,2008年经由欧洲航

天局PROBA-2卫星发射^[142],其同时监测4个选定紫外通道的太阳辐照度(探测器加上特定滤光片),时间分辨率低至10 ms^[142],将首次揭示太阳VUV辐射通量的亚秒结构。LYRA是第一个在太空中使用金刚石探测器的太阳物理仪器,如图8(c)~(g)所示^[142-145]。该探测器由比利时、日本和德国联合开发。他们制备了MSM结构^[145]和PIN结构^[143]的金刚石极紫外探测器。器件的极紫外性能测试在德国物理技术联邦研究中心的电子存储环BESSY II上进行。测试结果表明,金刚石探测器显示出极低的暗电流(pA量级)、大于4个量级的可见抑制比(200 nm versus 500 nm)和极紫外范围内的良好响应度^[142]。此外,为了探测特定的太阳极紫外光谱线,金刚石探测器和硅探测器需要与特定的滤光片结合,包括17~80 nm波长范围内的铝(Al)滤光片和6~20 nm波长范围内的锆(Zr)滤光片^[142]。图8(h)和图8(i)显示了LYRA中铝滤光片-探测器组合以及锆滤光片-探测器组合的绝对光谱响应度。在最终集成到PROBA-2之前,LYRA在VUV光谱范围的响应度、线性度、稳定性和均匀性等性能都需要进行测量和校准。经过测试校准,LYRA的4个通道都具有良好的均匀性、线性度、长期稳定性以及极低的暗电流。

3 总 结

本文综述了气体探测器、闪烁体、微通道板和半导体探测器在极紫外探测领域的应用和发展。图9列举了上述探测器的性能对比,以及各自适用的场景。气体探测器具有长期稳定性和优异的能量响应,已被用于FEL脉冲光子通量监测和宽光谱的绝对测量。在极紫外波段不可见辐射的检测和可视化方面,闪烁体可以将不可见辐射能量转化为可探测的光。其中Ce:YAG和水杨酸钠闪烁体已经实现了商业化,它们具有高的量子效率,但其面临辐射损伤导致性能退化的挑战。ZnO闪烁体可以实现皮秒级超快极紫外探测和成像,可用于极紫外源的泵浦、探针实验中。微通道板技术已经相对成熟,并且已被广泛应用于许多航天任务中的极紫外探测。硅探测器常被用作极紫外辐射的标准探测器,这得益于其较高的外部量子效率和成熟的制造工艺。然而,在强烈的极紫外辐射下,硅探测器容易受到辐射损伤,导致其探测性能和寿命下降。近20年来,基于宽禁带半导体的极紫外探测器因具有较强的耐辐照性而受到了越来越多研究人员的关注,代表性器件包括SiC、AlGaN和金刚石极紫外探测器。其中,金刚石极紫外探测器已被用于欧洲航天局的太阳辐射计LYRA系统中。然而,与硅极紫外探测器相比,宽禁带半导体极紫外探测器的制造技术尚不成熟,在未来的研究中需要投入更多的精力。

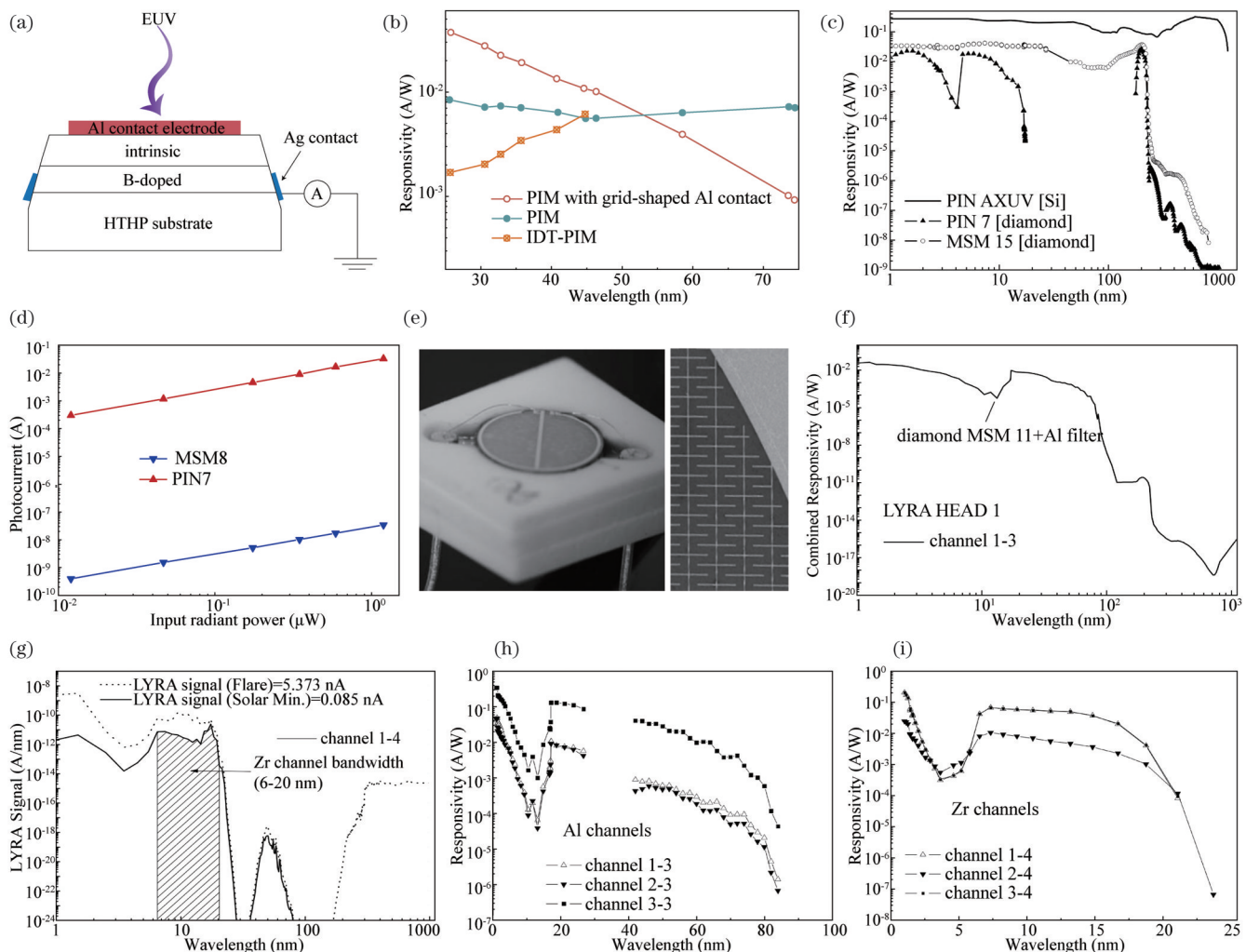


图 8 金刚石极紫外探测器的研究进展。(a)PIM 结构金刚石极紫外探测器结构图^[139];(b)两种具有不同接触几何形状的 PIM 结构金刚石极紫外探测器在 20~80 nm 光谱范围内的响应度^[139];(c)硅 AXUV 探测器、金刚石 PIN 和 MSM 探测器在 1~1000 nm 之间的光谱响应^[142];(d)金刚石 PIN 7 和 MSM 8 探测器在 200 nm 处的通量线性度及其拟合函数^[144];(e)MSM 和 Ti/Pt/Au 接触结构的细节^[142];(f) 1~1100 nm 波长范围内 LYRA 单元(MSM 11 探测器+铝滤光片)的模拟光谱响应度^[142];(g)通道 1~4 的 LYRA 辐射模型模拟示例^[142];(h)~(i)LYRA 中铝滤光片-探测器组合以及锆滤光片-探测器组合的绝对光谱响应度^[142]

Fig. 8 Research progress of the diamond-based EUV photodetectors. (a) Structural diagram of a PIM diamond-based EUV detector^[139]; (b) responsivity for PIM structure diamond-based EUV detectors with two different contact geometries in the spectral range of 20 to 80 nm^[139]; (c) spectral response of a silicon-based AXUV detector, diamond-based PIN and MSM detectors in the range of 1 to 1000 nm^[142]; (d) flux linearity at 200 nm for diamond-based PIN 7 and MSM 8 detectors, along with their fitting functions^[144]; (e) details of the MSM and Ti/Pt/Au contact structures^[142]; (f) simulated spectral responsivity of the LYRA unit (MSM 11 detector + Al filter) between 1 and 1100 nm^[142]; (g) simulation example of LYRA radiation model for channel 1-4^[142]; (h)–(i) absolute spectral responsivity of the Al filter-detector combination and the Zr filter-detector combination in LYRA^[142]

4 展望

4.1 耐辐照极紫外功率监测

极紫外功率计能对极紫外光刻光源和曝光的光功率进行准确测量,从而保证极紫外光刻工艺的可靠性和精度,是极紫外光刻系统开发的重要组成部分。目前,主流的极紫外功率计是硅半导体极紫外探测器。然而,极紫外光刻使用的极紫外光源具有极高的能量密度,会使功率计因辐射损伤而老化。如何提高功率

计的耐辐照能力是当前亟待解决的问题。这一需求使研究者们将目光投向了宽禁带半导体材料。然而,当前的宽禁带半导体极紫外探测器仍然主要集中在科学的研究方面,这与其尚未成熟的材料和器件制备工艺有关。目前其面临的挑战包括高质量大尺寸单晶衬底生长技术、外延薄膜生长技术以及掺杂技术。这也是宽禁带半导体微电子和光电子器件未来发展的方向。不过,相信随着宽禁带半导体器件技术的不断发展,宽禁带半导体极紫外功率计将在性能提升、使用寿命



图 9 极紫外探测所用的气体探测器、闪烁体、微通道板、硅探测器和宽禁带半导体探测器的性能对比

Fig. 9 Performance comparison of gas monitor detectors, scintillators, microchannel plates, silicon-based photodetectors and wide-bandgap semiconductor-based photodetectors for EUV photodetection

命和工艺重复等方面不断取得突破,有望为高制程半导体制造工艺提供有力支持。

4.2 高分辨极紫外成像

极紫外成像技术可以实现纳米尺度的分辨能力,相比电子显微镜来说,具有无损和快速成像的优势,非常适合芯片检测和生物光子学研究。目前,极紫外显微镜中主要使用的是硅基 CCD,其在极紫外波段不耐辐照且会受到可见光干扰。宽禁带半导体探测器可以避开上述限制。然而,目前大部分工作还停留在实验室阶段,集成度低。未来需要开发先进的宽禁带半导体探测阵列集成工艺,实现超过 1024×1024 的像素集成,并针对性设计适合宽带半导体探测阵列的高速读出电路,实现高分辨极紫外成像。

4.3 高抑制比极紫外微光探测

人们对宇宙中极紫外探测的需求与兴趣正日益增长。由于缺乏极紫外带通滤光片,传统的半导体探测器无法在强背景光下同时实现非极紫外光抑制和极紫外微光探测。理论上,基于超宽禁带半导体的雪崩探测器天然具有超过 4 个量级的极紫外/可见光抑制比,同时还能通过提升反偏电压实现超高的光电离内部增益,在高抑制比极紫外微光探测领域极具潜力。目前,针对极紫外波段的雪崩探测器研究还鲜有报道。未来,超宽禁带半导体雪崩探测器将成为本领域的研究重点,而超宽禁带半导体的高质量外延和可控掺杂则是需要面对的重要挑战。

参 考 文 献

- [1] Zheng W, Jia L M, Huang F. Vacuum-ultraviolet photon detections[J]. iScience, 2020, 23(6): 101145.
- [2] Jia L M, Zheng W, Huang F. Vacuum-ultraviolet photodetectors [J]. Photonix, 2020, 1(1): 22.
- [3] Hofman S. ASML wins SEMI Americas award for EUV lithography[EB/OM]. (2020-07-20) [2023-12-20]. <https://www.asml.com/en/news/stories/2020/asml-wins-semi-americas-award-for-euv>.
- [4] 李镇广, 窦银萍, 谢卓, 等. 结构锡靶激光等离子体极紫外光辐射特性研究[J]. 中国激光, 2021, 48(16): 1601005.
- [5] Li Z G, Dou Y P, Xie Z, et al. Characteristics of extreme ultraviolet emission from laser-produced plasma on structured Sn target[J]. Chinese Journal of Lasers, 2021, 48(16): 1601005.
- [6] Naulleau P P, Gargini P A, Itani T, et al. Extreme ultraviolet lithography 2020[J]. Proceedings of SPIE, 2020, 11517: 1151719.
- [7] Rice B J. Extreme ultraviolet (EUV) lithography[M] // Nanolithography. Amsterdam: Elsevier, 2014: 42-79.
- [8] Silverman P J. Extreme ultraviolet lithography: overview and development status[J]. Journal of Micro/Nanolithography, MEMS, and MOEMS, 2005, 4(1): 011006.
- [9] Wu B Q, Kumar A. Extreme ultraviolet lithography: a review[J]. Journal of Vacuum Science & Technology B: Microelectronics and Nanometer Structures Processing, Measurement, and Phenomena, 2007, 25(6): 1743-1761.
- [10] Takase K, Kamaji Y, Sakagami N, et al. Imaging performance improvement of an extreme ultraviolet microscope[J]. Japanese Journal of Applied Physics, 2010, 49(6S): 06GD07.
- [11] Terasawa T, Yamane T, Tanaka T, et al. Actinic mask blank inspection and signal analysis for detecting phase defects down to 1.5 nm in height[J]. Japanese Journal of Applied Physics, 2009, 48 (6S): 06FA04.
- [12] Neuhäusler U, Oelsner A, Slieh J, et al. High-resolution actinic defect inspection for extreme ultraviolet lithography multilayer mask blanks by photoemission electron microscopy[J]. Applied Physics Letters, 2006, 88(5): 053113.
- [13] Booth M, Brisco O, Brunton A, et al. High-resolution EUV imaging tools for resist exposure and aerial image monitoring[J]. Proceedings of SPIE, 2005, 5751: 78-89.
- [14] Nishimoto S, Watanabe K, Kawai T, et al. Validation of computed extreme ultraviolet emission spectra during solar ares[J]. Earth, Planets and Space, 2021, 73(1): 79.
- [15] Woods T N, Eparvier F G, Hock R, et al. Extreme ultraviolet variability experiment (EVE) on the solar dynamics observatory

- (SDO): overview of science objectives, instrument design, data products, and model developments[M]//Chamberlin P, Pesnell W D, Thompson B. The solar dynamics observatory. New York: Springer, 2010: 115-143.
- [15] Murchikova L, Murphy E J, LIS D C, et al. Reconstructing the EUV spectrum of star-forming regions from millimeter recombination lines of H I, He I, and He II[J]. *The Astrophysical Journal*, 2020, 903(1): 29.
- [16] Bowyer S, Jelinsky P, Christian C, et al. The extreme ultraviolet explorer mission[J]. *Highlights of Astronomy*, 2016, 9: 247-254.
- [17] Schmidtko G, Nikutowski B, Jacobi C, et al. Solar EUV irradiance measurements by the auto-calibrating EUV spectrometers (SolACES) aboard the international space station (ISS)[J]. *Solar Physics*, 2014, 289(5): 1863-1883.
- [18] Dere K P. Extreme ultraviolet spectra of solar active regions and their analysis[J]. *Solar Physics*, 1982, 77(1): 77-93.
- [19] Hans A, Schmidt P, Ozga C, et al. Extreme ultraviolet to visible dispersed single photon detection for highly sensitive sensing of fundamental processes in diverse samples[J]. *Materials*, 2018, 11(6): 869.
- [20] Sasaki A, Sunahara A, Nishihara K, et al. Atomic modeling of the plasma EUV sources[J]. *High Energy Density Physics*, 2007, 3(1/2): 250-255.
- [21] Dattoli G, Doria A, Gallerano G P, et al. Extreme ultraviolet (EUV) sources for lithography based on synchrotron radiation[J]. *Nuclear Instruments and Methods in Physics Research Section A: Accelerators, Spectrometers, Detectors and Associated Equipment*, 2001, 474(3): 259-272.
- [22] Lebert R, Bergmann K, Schriever G, et al. A gas discharged based radiation source for EUV-lithography[J]. *Microelectronic Engineering*, 1999, 46(1/2/3/4): 449-452.
- [23] Nakamura N, Kato R, Sakai H, et al. High-power EUV free-electron laser for future lithography[J]. *Japanese Journal of Applied Physics*, 2023, 62(SG): SG0809.
- [24] Yu Y, Li Q M, Yang J Y, et al. Dalian extreme ultraviolet coherent light source[J]. *Chinese Journal of Lasers*, 2019, 46(1): 0100005.
- [25] Bartnik A, Fiedorowicz H, Jarocki R, et al. Laser-plasma EUV source dedicated for surface processing of polymers[J]. *Nuclear Instruments and Methods in Physics Research Section A: Accelerators, Spectrometers, Detectors and Associated Equipment*, 2011, 647(1): 125-131.
- [26] Ahad I U, Bartnik A, Fiedorowicz H, et al. Surface modification of polymers for biocompatibility via exposure to extreme ultraviolet radiation[J]. *Journal of Biomedical Materials Research Part A*, 2014, 102(9): 3298-3310.
- [27] Zürch M, Foertsch S, Matzas M, et al. Cancer cell classification with coherent diffraction imaging using an extreme ultraviolet radiation source[J]. *Journal of Medical Imaging*, 2014, 1(3): 031008.
- [28] Liu C, Eschen W, Loetgering L, et al. Visualizing the ultrastructure of microorganisms using table-top extreme ultraviolet imaging[J]. *Photonix*, 2023, 4(1): 6.
- [29] Barkusky F, Bayer A, Döring S, et al. Damage threshold measurements on EUV optics using focused radiation from a table-top laser produced plasma source[J]. *Optics Express*, 2010, 18(5): 4346-4355.
- [30] Pearton S J, Aitkaliyeva A, Xian M H, et al. Review: radiation damage in wide and ultra-wide bandgap semiconductors[J]. *ECS Journal of Solid State Science and Technology*, 2021, 10(5): 055008.
- [31] Zhu S Q, Lin Z G, Wang Z, et al. Vacuum-ultraviolet ($\lambda < 200$ nm) photodetector array[J]. *Photonix*, 2024, 5(1): 5.
- [32] Moeller S, Brown G, Dakovski G, et al. Pulse energy measurement at the SXR instrument[J]. *Journal of Synchrotron Radiation*, 2015, 22(3): 606-611.
- [33] Sorokin A A. Gas-monitor detector for intense and pulsed VUV/EUV free-electron laser radiation[C]. *AIP Conference Proceedings*, 2004, 705: 557-560.
- [34] Richter M, Gottwald A, Kroth U, et al. Measurement of gigawatt radiation pulses from a vacuum and extreme ultraviolet free-electron laser[J]. *Applied Physics Letters*, 2003, 83(14): 2970-2972.
- [35] Kirschner H, Kaser H, Gottwald A. Commissioning of a gas monitor detector for an undulator beamline in the VUV and EUV wavelength range[J]. *Journal of Physics: Conference Series*, 2022, 2380(1): 012084.
- [36] Samson J A R. Absolute intensity measurements in the vacuum ultraviolet[J]. *Journal of the Optical Society of America*, 1964, 54(1): 6-15.
- [37] Samson J A R, Haddad G N. Absolute photon-flux measurements in the vacuum ultraviolet[J]. *Journal of the Optical Society of America*, 1974, 64(1): 47-54.
- [38] Saito N, Suzuki I H. Absolute soft X-ray measurements using an ion chamber[J]. *Journal of Synchrotron Radiation*, 1998, 5(3): 869-871.
- [39] Saito N, Suzuki I H. Absolute fluence rates of soft X-rays using a double ion chamber[J]. *Journal of Electron Spectroscopy and Related Phenomena*, 1999, 101/102/103: 33-37.
- [40] Sorokin A A, Bican Y, Bonfigt S, et al. An X-ray gas monitor for free-electron lasers[J]. *Journal of Synchrotron Radiation*, 2019, 26(4): 1092-1100.
- [41] Tiedtke K, Feldhaus J, Hahn U, et al. Gas detectors for X-ray lasers[J]. *Journal of Applied Physics*, 2008, 103(9): 094511.
- [42] Bobashev S V, Shmaenok L A. Photoionization quantometer for absolute intensity measurements of vacuum ultraviolet and soft X-ray radiation from laser plasma[J]. *Review of Scientific Instruments*, 1981, 52(1): 16-20.
- [43] Braune M, Brenner G, Dzirarhytski S, et al. A non-invasive online photoionization spectrometer for FLASH 2[J]. *Journal of Synchrotron Radiation*, 2016, 23(1): 10-20.
- [44] Faatz B, Plönjes E, Ackermann S, et al. Simultaneous operation of two soft X-ray free-electron lasers driven by one linear accelerator[J]. *New Journal of Physics*, 2016, 18(6): 062002.
- [45] Grünert J, Carbonell M P, Dietrich F, et al. X-ray photon diagnostics at the European XFEL[J]. *Journal of Synchrotron Radiation*, 2019, 26(Pt 5): 1422-1431.
- [46] Juranić P, Rehanek J, Arrell C A, et al. SwissFEL Aramis beamline photon diagnostics[J]. *Journal of Synchrotron Radiation*, 2018, 25(4): 1238-1248.
- [47] Maltezopoulos T, Dietrich F, Freund W, et al. Operation of X-ray gas monitors at the European XFEL[J]. *Journal of Synchrotron Radiation*, 2019, 26(Pt 4): 1045-1051.
- [48] Song S, Alonso-Mori R, Chollet M, et al. Measurement of the absolute number of photons of the hard X-ray beamline at the Linac Coherent Light Source[J]. *Journal of Synchrotron Radiation*, 2019, 26(2): 320-327.
- [49] Burian T, Hájková V, Chalupský J, et al. Soft X-ray free-electron laser induced damage to inorganic scintillators[J]. *Optical Materials Express*, 2015, 5(2): 254-264.
- [50] Liu Z Y, Liu S, Wang K, et al. Measurement and numerical studies of optical properties of YAG: Ce phosphor for white light-emitting diode packaging[J]. *Applied Optics*, 2010, 49(2): 247-257.
- [51] Krzywinski J, Andrejczuk A, Bionta R M, et al. Saturation of a Ce: $Y_3Al_5O_{12}$ scintillator response to ultra-short pulses of extreme ultraviolet soft X-ray and X-ray laser radiation[J]. *Optical Materials Express*, 2017, 7(3): 665-675.
- [52] Bahrenberg L, Herbert S, Mathmann T, et al. Design of structured YAG: Ce scintillators with enhanced outcoupling for image detection in the extreme ultraviolet[J]. *Optics Letters*, 2017, 42(19): 3848-3851.
- [53] Szilagyi J M. Extreme ultraviolet spectral streak camera[D]. Orlando: University of Central Florida, 2010: 1682.
- [54] Baciero A, Placentino L, McCarthy K J, et al. Vacuum ultraviolet

- and X-ray luminescence efficiencies of $\text{Y}_3\text{Al}_5\text{O}_{12}:\text{Ce}$ phosphor screens[J]. Journal of Applied Physics, 1999, 85(9): 6790-6796.
- [55] Baciero A, McCarthy K J, Acedo M A, et al. A study of the response of $\text{Y}_3\text{Al}_5\text{O}_{12}:\text{Ce}$ phosphor powder screens in the vacuum ultraviolet and soft X-ray regions using synchrotron radiation[J]. Journal of Synchrotron Radiation, 2000, 7(4): 215-220.
- [56] Benk M, Bergmann K. Adaptive spatially resolving detector for the extreme ultraviolet with absolute measuring capability[J]. The Review of Scientific Instruments, 2009, 80(3): 033113.
- [57] Chai K B, Bellan P M. Extreme ultra-violet movie camera for imaging microsecond time scale magnetic reconnection[J]. The Review of Scientific Instruments, 2013, 84(12): 123504.
- [58] Yang T I, Hui Y Y, Lo J I, et al. Imaging extreme ultraviolet radiation using nanodiamonds with nitrogen-vacancy centers[J]. Nano Letters, 2023, 23(21): 9811-9816.
- [59] Tanaka M, Nishikino M, Yamatani H, et al. Hydrothermal method grown large-sized zinc oxide single crystal as fast scintillator for future extreme ultraviolet lithography[J]. Applied Physics Letters, 2007, 91(23): 231117.
- [60] Furukawa Y, Tanaka M, Nakazato T, et al. Temperature dependence of scintillation properties for a hydrothermal-method-grown zinc oxide crystal evaluated by nickel-like silver laser pulses [J]. Journal of the Optical Society of America B, 2008, 25(7): B118-B121.
- [61] Nakazato T, Furukawa Y, Tanaka M, et al. Hydrothermal-method-grown ZnO single crystal as fast EUV scintillator for future lithography[J]. Journal of Crystal Growth, 2009, 311(3): 875-877.
- [62] Furukawa Y, Tanaka M, Nishikino M, et al. UV fluorescence of hydrothermal method grown ZnO for fast EUV scintillators[C]// 2008 Conference on Lasers and Electro-Optics and 2008 Conference on Quantum Electronics and Laser Science, May 4-9, 2008, San Jose, CA, USA. New York: IEEE Press, 2008.
- [63] Yamanoi K, Sakai K, Nakazato T, et al. Response-time improved hydrothermal-method-grown ZnO scintillator for XFEL timing-observation[J]. Optical Materials, 2010, 32(10): 1305-1308.
- [64] Yamanoi K, Sakai K, Cadatal-Raduban M, et al. Indium-doped ZnO scintillator with 3-ps response time for accurate synchronization of optical and X-ray free electron laser pulses[J]. IEEE Transactions on Nuclear Science, 2012, 59(5): 2298-2300.
- [65] Shimizu T, Yamanoi K, Estacio E, et al. Response-time improved hydrothermal-method-grown ZnO scintillator for soft X-ray free-electron laser timing-observation[J]. The Review of Scientific Instruments, 2010, 81(3): 033102.
- [66] Lin R C, Zhu Y M, Chen L, et al. Ultrafast (600 ps) α -ray scintillators[J]. Photonix, 2022, 3(1): 9.
- [67] Kano M, Wakamiya A, Yamanoi K, et al. Fabrication of in-doped ZnO scintillator mounted on a vacuum flange[J]. IEEE Transactions on Nuclear Science, 2012, 59(5): 2290-2293.
- [68] Arita R, Nakazato T, Shimizu T, et al. High spatial resolution ZnO scintillator for an *in situ* imaging device in EUV region[J]. Optical Materials, 2014, 36(12): 2012-2015.
- [69] Nakazato T, Hori T, Shimizu T, et al. Spatial resolution evaluation of ZnO scintillator as an *in-situ* imaging device in EUV region[J]. IEEE Transactions on Nuclear Science, 2014, 61(1): 462-466.
- [70] Watanabe K, Inn E C Y. Intensity measurements in the vacuum ultraviolet[J]. Journal of the Optical Society of America, 1953, 43(1): 32-35.
- [71] McKinsey D N, Brome C R, Butterworth J S, et al. Fluorescence efficiencies of thin scintillating films in the extreme ultraviolet spectral region[J]. Nuclear Instruments and Methods in Physics Research Section B: Beam Interactions with Materials and Atoms, 1997, 132(3): 351-358.
- [72] Samson J A R, Cairns R B. A carbon film-scintillator combination suitable for the selective detection of radiation in the extreme ultraviolet[J]. Applied Optics, 1965, 4(8): 915-916.
- [73] Bruner E C. Absolute quantum efficiency of sodium salicylate for excitation by extreme ultraviolet[J]. Journal of the Optical Society of America, 1969, 59(2): 204-211.
- [74] Iglesias E J, Mitschke F, Fiebrandt M, et al. *In situ* measurement of VUV/UV radiation from low-pressure microwave-produced plasma in Ar/O₂ gas mixtures[J]. Measurement Science and Technology, 2017, 28(8): 085501.
- [75] Han J, Park W, Mauchaffé R, et al. Real-time VUV radiation monitoring in low-pressure hydrogen plasma based on fluorescence of sodium salicylate[J]. Measurement Science and Technology, 2023, 34(2): 025006.
- [76] Kumar V, Datta A K. Vacuum ultraviolet scintillators: sodium salicylate and p-terphenyl[J]. Applied Optics, 1979, 18(9): 1414-1417.
- [77] Model 658 end-on PMT housing assembly[EB/OL]. [2023-11-12]. <https://www.mcpheeisoninc.com/detectors/model650detectorassembly.html>.
- [78] Yang T I, Azuma T, Huang Y W, et al. Stimulated emission cross sections and temperature-dependent spectral shifts of neutral nitrogen-vacancy centers in diamonds[J]. Journal of the Chinese Chemical Society, 2023, 70(3): 451-459.
- [79] Lu H C, Lo J I, Peng Y C, et al. Photoluminescence of diamond containing nitrogen vacancy defects as a sensor of temperature upon exposure to vacuum- and extreme-ultraviolet radiation[J]. Physical Chemistry Chemical Physics, 2020, 22(46): 26982-26986.
- [80] Lu H C, Lo J I, Peng Y C, et al. Nitrogen-vacancy centers in diamond for high-performance detection of vacuum ultraviolet, extreme ultraviolet, and X-rays[J]. ACS Applied Materials & Interfaces, 2020, 12(3): 3847-3853.
- [81] Siegmund O H W, Malina R F. Detection of extreme UV and soft X-rays with microchannel plates: a review[M] // Talmi Y. Multichannel image detectors volume 2. Washington, DC: American Chemical Society, 1983: 253-275.
- [82] Tremsin A S, McPhate J B, Steuwer A, et al. High-resolution strain mapping through time-of-flight neutron transmission diffraction with a microchannel plate neutron counting detector[J]. Strain, 2012, 48(4): 296-305.
- [83] Laprade B N, Dykstra M W, Langevin F. Development of an ultrasmall-pore microchannel plate for space sciences applications [J]. Proceedings of SPIE, 1996, 2808: 72-85.
- [84] Demarest J A, Watson R L. Beam-foil spectroscopy in the EUV employing a position sensitive microchannel plate[J]. Nuclear Instruments and Methods in Physics Research Section B: Beam Interactions with Materials and Atoms, 1987, 24/25: 296-300.
- [85] Fraser G W. Imaging detectors for FUV and EUV wavelengths[J]. Advances in Space Research, 1991, 11(11): 155-166.
- [86] Vallerga J V, Siegmund O H W, Vedder P W, et al. Investigations of the small-scale flat field response of microchannel plate detectors in the far and extreme ultraviolet[J]. Nuclear Instruments and Methods in Physics Research Section A: Accelerators, Spectrometers, Detectors and Associated Equipment, 1991, 310(1/2): 317-322.
- [87] Tremsin A S, Jelinsky S R, Siegmund O H W. Quantum efficiency and spatial resolution of microsphere plates stacked with microchannel plates[J]. Proceedings of SPIE, 1997, 3114: 272-282.
- [88] Lapington J S. Developments in imaging devices for microchannel plate detectors[J]. Proceedings of SPIE, 2003, 4854: 191-202.
- [89] Bannister N P, Lapington J S, Barstow M A, et al. High-resolution imaging microchannel plate detector for EUV spectrometry[J]. Proceedings of SPIE, 2000, 4140: 199-210.
- [90] Pfeifer M, Barnstedt J, Diebold S, et al. Characterisation of low power readout electronics for a UV microchannel plate detector with cross-strip readout[J]. Proceedings of SPIE, 2014, 9144: 914438.
- [91] Sandel B R, Broadfoot A L, Curtis C C, et al. The extreme ultraviolet imager investigation for the image mission[M] // Burch J

- L. The image mission. Dordrecht: Springer, 2000: 197-242.
- [92] Miao Z H. A single photon system based on wedge and strip anodes detector[D]. Xi'an: Xi'an Institute of Optics and Precision Mechanics, Chinese Academy of Sciences, 2009.
- [93] 尼启良. 极紫外微通道板光子计数成像探测器性能研究[J]. 光学学报, 2013, 33(11): 1104001.
- Ni Q L. Study on characteristic performance of a MCP-based photon-counting imaging detector[J]. Acta Optica Sinica, 2013, 33(11): 1104001.
- [94] Zhu X P, Zhao B S, Liu Y A, et al. Experimental study on 30.4 nm extreme ultraviolet imaging detector[J]. Acta Optica Sinica, 2008, 28(10): 1925-1929.
- [95] Bu S F, Ni Q L, He L P, et al. Microchannel plate photon counting detector in UV range[J]. Chinese Journal of Optics and Applied Optics, 2012, 5(3): 302-309.
- [96] Stock J M, Siegmund O H W, Hurwitz M, et al. Berkeley EUV spectrometer microchannel plate detectors for ORFEUS[J]. Proceedings of SPIE, 1993, 2006: 128-138.
- [97] Pfeifer M, Barnstedt J, Bauer C, et al. Low-power readout electronics for micro channel plate detectors with cross-strip anodes [J]. Proceedings of SPIE, 2012, 8443: 84432O.
- [98] Schindhelm E R, Green J C, Siegmund O H W, et al. Microchannel plate detector technology potential for LUVOIR and HabEx[J]. Proceedings of SPIE, 2017, 10397: 1039711.
- [99] Ertley C, Siegmund O, Vallerga J, et al. Microchannel plate detectors for future NASA UV observatories[J]. Proceedings of SPIE, 2018, 10699: 106993H.
- [100] Siegmund O H W, Vallerga J V, Darling N T, et al. UV imaging detectors with high performance microchannel plates[J]. Proceedings of SPIE, 2019, 11118: 11118N.
- [101] 微通道板 (MCP) 原理及重要参数介绍 [EB/OL]. [2023-11-12]. <http://share.hamamatsu.com.cn/specialDetail/1087.html>. Introduction to the principle and important parameters of microchannel panel (MCP) [EB/OL]. [2023-11-12]. <http://share.hamamatsu.com.cn/specialDetail/1087.html>.
- [102] Korde R, Cable J S, Canfield L R. One gigarad passivating nitrided oxides for 100% internal quantum efficiency silicon photodiodes[J]. IEEE Transactions on Nuclear Science, 1993, 40(6): 1655-1659.
- [103] Canfield L R, Kerner J A, Korde R S. Silicon photodiodes optimized for the EUV and soft X-ray regions[J]. Proceedings of SPIE, 1990, 1344: 372-377.
- [104] Hartmann R, Hauff D, Lechner P, et al. Low energy response of silicon pn-junction detector[J]. Nuclear Instruments and Methods in Physics Research Section A: Accelerators, Spectrometers, Detectors and Associated Equipment, 1996, 377(2/3): 191-196.
- [105] Šakić A, Nanver L K, Scholtes T L M, et al. Boron-layer silicon photodiodes for high-efficiency low-energy electron detection[J]. Solid State Electronics, 2011, 65/66: 38-44.
- [106] Shi L, Sarubbi F, Nihtianov S N, et al. High performance silicon-based extreme ultraviolet (EUV) radiation detector for industrial application[C]//2009 35th Annual Conference of IEEE Industrial Electronics, November 3-5, 2009, Porto, Portugal. New York: IEEE Press, 2009: 1877-1882.
- [107] Shi L, Nihtianov S, Nanver L K, et al. Stability characterization of high-sensitivity silicon-based EUV photodiodes in a detrimental environment[J]. IEEE Sensors Journal, 2013, 13(5): 1699-1707.
- [108] Aruev P N, Barysheva M M, Ber B Y, et al. Silicon photodiode with selective Zr/Si coating for extreme ultraviolet spectral range [J]. Quantum Electronics, 2012, 42(10): 943-948.
- [109] Photodiodes: electron, photon, X-ray detectors (AXUV)[EB/OL]. [2023-11-12]. <https://optodiode.com/photodiodes-axuv-detectors.html>.
- [110] Photodiodes: EUV enhanced detectors (SXUV)[EB/OL]. [2023-11-12]. <https://optodiode.com/photodiodes-sxuv-detectors.html>.
- [111] Edmond J A, Kong H S, Carter C H, Jr. Blue LEDs, UV photodiodes and high-temperature rectifiers in 6H-SiC[J]. Physica B: Condensed Matter, 1993, 185(1/2/3/4): 453-460.
- [112] Yan F, Qin C, Zhao J H, et al. Low-noise visible-blind UV avalanche photodiodes with edge terminated by 2° positive bevel[J]. Electronics Letters, 2002, 38(7): 335-336.
- [113] Guo X, Beck A, Yang B, et al. Low dark current 4H-SiC avalanche photodiodes[J]. Electronics Letters, 2003, 39(23): 1-2.
- [114] Yan F, Xin X B, Aslam S, et al. 4H-SiC UV photo detectors with large area and very high specific detectivity[J]. IEEE Journal of Quantum Electronics, 2004, 40(9): 1315-1320.
- [115] Xin X, Yan F, Koeth T W, et al. Demonstration of 4H-SiC visible-blind EUV and UV detector with large detection area[J]. Electronics Letters, 2005, 41(21): 1192-1193.
- [116] Torrisi A, Wachulak P, Fiedorowicz H, et al. Silicon carbide detectors for diagnostics of laser-produced plasmas[J]. Proceedings of SPIE, 2019, 11032: 110320W.
- [117] Seely J F, Kjornrattanawanich B, Holland G E, et al. Response of a SiC photodiode to extreme ultraviolet through visible radiation[J]. Optics Letters, 2005, 30(23): 3120-3122.
- [118] Torrisi A, Wachulak P W, Fiedorowicz H, et al. SiC detectors for evaluation of laser-plasma dynamics employing gas-puff targets[J]. Nuclear Instruments and Methods in Physics Research Section A: Accelerators, Spectrometers, Detectors and Associated Equipment, 2019, 922: 250-256.
- [119] Torrisi A, Wachulak P, Fiedorowicz H, et al. Characterization of Si and SiC detectors for laser-generated plasma monitoring in short wavelength range[J]. Journal of Instrumentation, 2020, 15(5): C05027.
- [120] Gottwald A, Kroth U, Kalinina E, et al. Optical properties of a Cr/4H-SiC photodetector in the spectral range from ultraviolet to extreme ultraviolet[J]. Applied Optics, 2018, 57(28): 8431-8436.
- [121] Hu J, Xin X B, Joseph C L, et al. 1×16 Pt/4H-SiC Schottky photodiode array for low-level EUV and UV spectroscopic detection[J]. IEEE Photonics Technology Letters, 2008, 20(24): 2030-2032.
- [122] Wang Z Y, Zhou D, Xu W Z, et al. 4H-SiC δ n-i-p extreme ultraviolet detector with gradient doping-induced surface junction [J]. IEEE Electron Device Letters, 2022, 43(6): 906-909.
- [123] Zhang R J, Liu J, Liu G, et al. A dual P-layer 4H-SiC p-i-n photodetector for the detection from extreme ultraviolet to ultraviolet-A[J]. Electronics Letters, 2023, 59(18): e12953.
- [124] Malinowski P E, Duboz J Y, de Moor P, et al. EUV detectors based on AlGaN-on-Si Schottky photodiodes[J]. Proceedings of SPIE, 2011, 8073: 807302.
- [125] Rogalski A, Bielecki Z, Mikołajczyk J, et al. Ultraviolet photodetectors: from photocathodes to low-dimensional solids[J]. Sensors, 2023, 23(9): 4452.
- [126] Malinowski P E, Duboz J Y, John J, et al. AlGaN-on-Si backside illuminated photodetectors for the extreme ultraviolet (EUV) range [J]. Proceedings of SPIE, 2010, 7726: 772617.
- [127] Malinowski P E, Duboz J Y, de Moor P, et al. AlGaN-on-Si-based 10- μ m pixel-to-pixel pitch hybrid imagers for the EUV range [J]. IEEE Electron Device Letters, 2011, 32(11): 1561-1563.
- [128] Malinowski P E, Duboz J Y, de Moor P, et al. Extreme ultraviolet detection using AlGaN-on-Si inverted Schottky photodiodes[J]. Applied Physics Letters, 2011, 98(14): 141104.
- [129] Barkusky F, Peth C, Bayer A, et al. Radiation damage resistance of AlGaN detectors for applications in the extreme-ultraviolet spectral range[J]. The Review of Scientific Instruments, 2009, 80(9): 093102.
- [130] Malinowski P E, John J, Barkusky F, et al. Radiation hardness of $Al_xGa_{1-x}N$ photodetectors exposed to extreme ultraviolet (EUV) light beam[J]. Proceedings of SPIE, 2009, 7361: 73610T.
- [131] Cai Q, You H F, Guo H, et al. Progress on AlGaN-based solar-blind ultraviolet photodetectors and focal plane arrays[J]. Light, Science & Applications, 2021, 10(1): 94.
- [132] Reverchon J L, Bansropun S, Robo J A, et al. First demonstration and performance of AlGaN based focal plane array

- for deep-UV imaging[J]. Proceedings of SPIE, 2009, 7474: 74741G.
- [133] Reverchon J L, Bansropun S, Truffer J P, et al. Performances of AlGaN-based focal plane arrays from 10 nm to 200 nm[J]. Proceedings of SPIE, 2010, 7691: 769109.
- [134] Malinowski P E, Duboz J Y, de Moor P, et al. 10 μ m pixel-to-pixel pitch hybrid backside illuminated AlGaN-on-Si imagers for solar blind EUV radiation detection[C] //2010 International Electron Devices Meeting, December 06-08, 2010, San Francisco, CA, USA. New York: IEEE Press, 2010.
- [135] Prestopino G, Santoni E, Verona C, et al. Diamond based Schottky photodiode for radiation therapy *in vivo* dosimetry[J]. Materials Science Forum, 2016, 879: 95-100.
- [136] Pace E, di Benedetto R, Scuderi S. Fast stable visible-blind and highly sensitive CVD diamond UV photodetectors for laboratory and space applications[J]. Diamond and Related Materials, 2000, 9 (3/4/5/6): 987-993.
- [137] Balducci A, de Sio A, Marinelli M, et al. Extreme UV single crystal diamond photodetectors by chemical vapor deposition[J]. Diamond and Related Materials, 2005, 14(11/12): 1980-1983.
- [138] Almaviva S, Marinelli M, Milani E, et al. Extreme UV photodetectors based on CVD single crystal diamond in a p-type/intrinsic/metal configuration[J]. Diamond and Related Materials, 2009, 18(1): 101-105.
- [139] Almaviva S, Marinelli M, Milani E, et al. Extreme UV single crystal diamond Schottky photodiode in planar and transverse configuration[J]. Diamond and Related Materials, 2010, 19(1): 78-82.
- [140] Ciancaglioni I, di Venanzio C, Marinelli M, et al. Influence of the metallic contact in extreme-ultraviolet and soft X-ray diamond based Schottky photodiodes[J]. Journal of Applied Physics, 2011, 110(5): 054513.
- [141] Hochedez J F, Bergonzo P, Castex M C, et al. Diamond UV detectors for future solar physics missions[J]. Diamond and Related Materials, 2001, 10(3/4/5/6/7): 673-680.
- [142] BenMoussa A, Dammasch I E, Hochedez J F, et al. Pre-flight calibration of LYRA, the solar VUV radiometer on board PROBA2[J]. Astronomy & Astrophysics, 2009, 508(2): 1085-1094.
- [143] Benmoussa A, Schühle U, Haenen K, et al. PIN diamond detector development for LYRA, the solar VUV radiometer on board PROBA II[J]. Physica Status Solidi (a), 2004, 201(11): 2536-2541.
- [144] BenMoussa A, Hochedez J F, Schühle U, et al. Diamond detectors for LYRA, the solar VUV radiometer on board PROBA2[J]. Diamond and Related Materials, 2006, 15(4/5/6/7/8): 802-806.
- [145] BenMoussa A, Theissen A, Scholze F, et al. Performance of diamond detectors for VUV applications[J]. Nuclear Instruments and Methods in Physics Research Section A: Accelerators, Spectrometers, Detectors and Associated Equipment, 2006, 568 (1): 398-405.

Extreme Ultraviolet Detectors: A Review

Zheng Wei*, Zhang Naiji, Zhu Sisi, Zhang Lixin, Cai Wei

State Key Laboratory of Optoelectronic Materials and Technologies, School of Materials, Sun Yat-sen University, Shenzhen 518107, Guangdong, China

Abstract

Significance Extreme ultraviolet (EUV) detectors play an irreplaceable role in the fields of electronics manufacturing, space exploration, and basic science research. In electronics manufacturing, EUV lithography offers new possibilities for realizing circuit patterns in smaller sizes. The application of EUV detectors in EUV lithography is crucial because reliable detectors in EUV lithography systems can realize accurate monitoring of light source power and exposure dose to ensure the accuracy and consistency of chip production. In space exploration, the EUV radiation released by solar activity changes the density and ionization of Earth's thermosphere and ionosphere, which will accordingly affect the performance of ground-based communication systems and spacecraft in low Earth orbit. EUV detectors can be effectively used to study solar activity, which can facilitate investigations on how solar changes affect Earth and technological systems in space missions, thereby improving the prediction capabilities. In basic science, as EUV light has a short wavelength and high energy, relevant studies of its characteristics and interaction mechanisms can deepen the understanding of the photon behavior and electronic structure of atoms and molecules. In this field, EUV detectors are a key component to calibrate the wavelength and intensity of light sources, providing a means to deeply explore the microstructure and basic laws of the material world (Fig. 1). Starting with the important application scenarios of EUV detectors in various fields, this review aims to provide a systematic introduction to the advantages and research progress of EUV detectors.

Progress As science and technology progress, various application scenarios have put forward different performance requirements for EUV detectors. This paper reviews the research progress of EUV detectors based on different detection media and working mechanisms, including the gas monitor detector (GMD), scintillator, micro-channel plate, and semiconductor-based photodetector.

GMDs can obtain information by detecting the ionization process after the absorption of EUV radiation. The stable real-time monitoring of the photon fluxes of high-power EUV light sources, such as synchrotron radiation and free-electron lasers (FEL), will affect subsequent tests, making the calibration of these light sources essential. Semiconductor diodes are typically used to measure the absolute photon fluxes; however, they may get damaged under high-power EUV radiation, increasing the uncertainty in EUV detection. In contrast, as GMDs can overcome the performance degradation induced by radiation and realize real-time monitoring of photon fluxes, it has been employed in several free electron laser devices (such as FLASH 2, SwissFEL, European XFEL, and LCLS II). Compared with the calibration of semiconductor diodes, GMDs have the advantages of low deviation, high stability, and long service life. Further, it is more effective in detecting high-power EUV radiation (Fig. 2).

Scintillators have been developed based on the down-conversion effect, which converts invisible EUV light into visible light to be collected by a back-end photodiode or photomultiplier tube. The scintillator is generally a fast and efficient photoluminescent material with sufficient size and is an ideal element for high-speed EUV detection and imaging. Scintillators exhibit high-yield luminescence, a fast response to EUV light, and a sufficiently high absorption coefficient. Ce:YAG, ZnO, and sodium salicylate are scintillators that have attracted significant attention in the field of EUV detection, among which the sodium salicylate scintillators have been commercialized (Fig. 3).

The micro-channel plate is a type of large-area electron multiplier detector that converts EUV photons into electrons through the external photoelectric effect that has the advantages of high spatial resolution and low noise. Micro-channel plate EUV detection technology has made great progress in the past few decades, including improvements in detection efficiency, response speed, and image reading technology. It has been widely used in the detection of the EUV band in aerospace missions, thus providing strong support for space science research. Micro-channel plates have been commercialized, mainly by the Hamamatsu Company (Fig. 4).

The semiconductor-based photodetector is a type of low-power miniaturized detector that utilizes the internal photoelectric effect. Its types include those based on silicon and wide-bandgap semiconductors, with the advantages of small size, light weight, and easy integration. Silicon-based photodetectors have been applied in a wide spectrum range, from X-rays to visible light, and the test data are considered the absolute calibration standard for EUV detection technology (Fig. 5). However, they are prone to face the problems of accelerated aging or even getting damaged under harsh conditions such as high temperatures and radiation. Considering the reliability and operating conditions of EUV detection, wide-bandgap semiconductor materials are preferred in such situations. Owing to its material characteristics, the EUV photodetector based on wide-bandgap semiconductors typically has a higher radiation damage threshold, stronger chemical and physical stability, and a lower intrinsic carrier concentration, which can ensure stable performance under high irradiation intensity. At present, some wide-bandgap semiconductor materials, such as SiC (Fig. 6), AlGaN (Fig. 7), and diamond (Fig. 8), have been used to manufacture EUV photodetectors. Detectors based on those materials have exhibited a longer service life under the same irradiation conditions and greater advantages in relation to EUV lithography light source power and dose monitoring when compared with silicon-based photodetectors. Therefore, wide-bandgap semiconductors have important research significance with the ability to provide new avenues for the development of EUV detection technology.

Conclusions and Prospects This paper introduces the development and research status of EUV detection of the GMD, scintillator, micro-channel plate, and semiconductor-based photodetector (with the advantages and disadvantages listed in Fig. 9), particularly focusing on the EUV photodetector based on wide-bandgap semiconductors. All these types of detectors have been constantly optimized to meet the needs of different application scenarios. A deeper understanding is expected to be achieved in the future by dealing with the unsolved scientific problems in current EUV detection technology, such as irradiation-resistant EUV power monitoring, high-resolution EUV imaging, and high-rejection-ratio detection for weak EUV light. This in-depth research will provide more advanced technical means or methods for electronics manufacturing, space exploration, and basic science to promote the development of related fields.

Key words detector; extreme ultraviolet; scintillator; gas monitor detector; wide-bandgap semiconductor